Dear Reviewer 1,

Thank you for your positive remarks and insightful comments on the paper. We appreciate the time and effort that you have dedicated to our manuscript. We have discussed your main technical suggestions and summarized the outcome below. The small editorial suggestions will be also incorporated in the revised manuscript, which will be uploaded in a later stage.

- Line 191-199: *Changed the sentences in this section according to your suggestions.*
- Line 194: Why a value of 2?
  We use a factor of 2 because at the surface, the up- and down-going waves are recorded at the same time. By the division by 2, the amplitude of the upgoing wave is retrieved. We will add a sentence in the updated manuscript.
- Line 245-246: Why is the relationship between HVSR and AF of most importance?
  The relationship between the HVSR A_0 and the AF is used to obtain an AF per class for the zonation map (Section 6.3). HVSR records are available throughout the country while the AF is not. These lines are rewritten for more clarity.
- Line 255: What are x1, x2 and x3?
  You have raised a good point here and accordingly in the new manuscript we changed the x1, x2, x3 to a,b,c to circumvent confusion with Cartesian coordinates. a,b and c are the three unknown coefficients to be fitted. This line is rephrased for more clarity.
- Line 265: Do you mean that the influence of this parameter is the least?
  Indeed, we mean the influence is less. But removed the sentence since it was in repetition with the next sentence.
- Line 363: According to you, what can explain such a discrepancy? What show for example the corresponding ETF?
  Thank you for pointing this out. Unfortunately, for this area we cannot compute an ETF since it is seismically quiet. With this example we like to point out that the GeoTOP model is a model, and interpolated between the data points. This adds extra uncertainty to the map, which is discussed in Section 6.3.
- Line 394: A word is missing.
  Thanks, yes here a word is missing. Added 'regional pattern'.

We hope we cover your comments and are willing to respond to any further questions and suggestions you may have.

Sincerely,

Janneke van Ginkel, Elmer Ruigrok, Jan Stafleu and Rien Herber

Dear Reviewer 2,

Thank you for your comments on the paper. We appreciate the time and effort that you have dedicated to our manuscript. We have carefully reviewed the manuscript and rephrased some sections to better communicate the main message. In the introduction, the structure of the article is more emphasized. The sites and earthquakes used for the calculations are presented in Figure 2. For interpretation and justification of the results, we included more details on the methods and the effect of the subsurface geology on amplification.

We have discussed your main scientific questions and summarized the outcome below. The editorial suggestions will be also incorporated in the revised manuscript, which will be uploaded in a later stage. We believe that with the incorporation of your suggestions, the manuscript has improved.

Response to main scientific questions:

- L165: What is the justification for setting the reference bedrock at 200 m depth? This hypothesis has been supported neither by the geological profile nor by geophysical measurement. Is the geology at 200 m depth same everywhere? Is there any shear-wave velocity profile that shows that the formation at 200 m depth can be characterized as rock?

  Thanks for pointing this out and it is a relevant thought. Indeed, in the Netherlands at 200 m depth there is no real solid rock. Generally, amplification is determined with respect to a reference bedrock, but such reference site does not exist in the Netherlands. Studies by e.g., Poggi et al. (2011) also derive a reference site that does not correspond to an actual bedrock site. It is defined as an (average) S-wave velocity profile. We further simplify the approach by taking the elastic conditions at 200 m depth in Groningen as a reference, from which we define amplification. Similar conditions can be found (at the same or other depths) in most of the Netherlands.

  We define reference conditions at depth with a shear-wave velocity of 500 m/s. These are the in-situ shear-wave velocity values that are found, on average, at 200 m depth, based on studies on the Groningen borehole network from Hofman et al. (2017) and Kruiver et al. (2017). Overall, the subsurface composition throughout the country is quite uniform at 200 m depth and consists of semi-consolidated clastics. The (relatively few) locations with deviating subsurface conditions are evaluated separately and clustered in class V. You raised a good point that the term 'rock' in line 169 is misleading here. Section 4.1 is rephrased for more clarity.

- The authors mention that "This depth and corresponding average shear-wave velocity forms the basis from which the site-response and corresponding amplification factors (AFs) are estimated in the next sections." Where is this shear-wave velocity defined? If the bedrock is defined without any justification, the estimation of amplification in the entire work becomes highly questionable. The authors did mention something about Groningen network.

However, they do not show the location of this network with respect to their data. It's also very unclear how the bedrock has been identified from the G-network. How can a Vs 500 m/s be characterized as rock condition? How can this be applicable to all sites, especially in the south where there are older formations?

Some of these questions are already answered in the previous comment about how we define the reference shear-wave velocity, using conditions as found at 200 m depth at stations of n the Groningen borehole network. The location of the Groningen network is shown in the updated version of Figure 2 (see figure next page).

Overall, the subsurface composition throughout the country is quite uniform at 200 m depth. At some locations similar conditions can be found at shallower depths. The locations where the reference subsurface conditions do not occur in the top few hundred meters are evaluated separately and clustered in Class V. For example in the very south of the Netherlands, Class V can be found.

- Figure 1: What does the geological map correspond to? Does it show the geology at the surface or at any specific depth? The figure does not show geographical coordinates.

  It is the geological map for the surface geology, we added this remark to the caption. Also, the coordinates have been added.

- The description of the geology seems a bit incomplete. Even though this work uses two 3D geological models, there is not enough discussion about the geology at depths (e.g., at the base of the Quaternary or below).

  Thanks for pointing this out. In Section 2, additional details of the geology at larger depths are provided.

- Figure 2: Lat/Lon should be shown at least for two points on both axes.

  Indeed, thanks. More lat/long coordinates are added to the figure.

- L 190: The AFs are calculated from the G-network but the location of this network has not been shown. Do the boreholes with SCPT belong to this network?

  For more clarity, we added a subfigure to Figure 2 showing the Groningen borehole network and the locations of the local earthquakes used for AF and ETF computations. The purple triangles are the locations with SCPTs available.

  Find below the updated figure and caption:

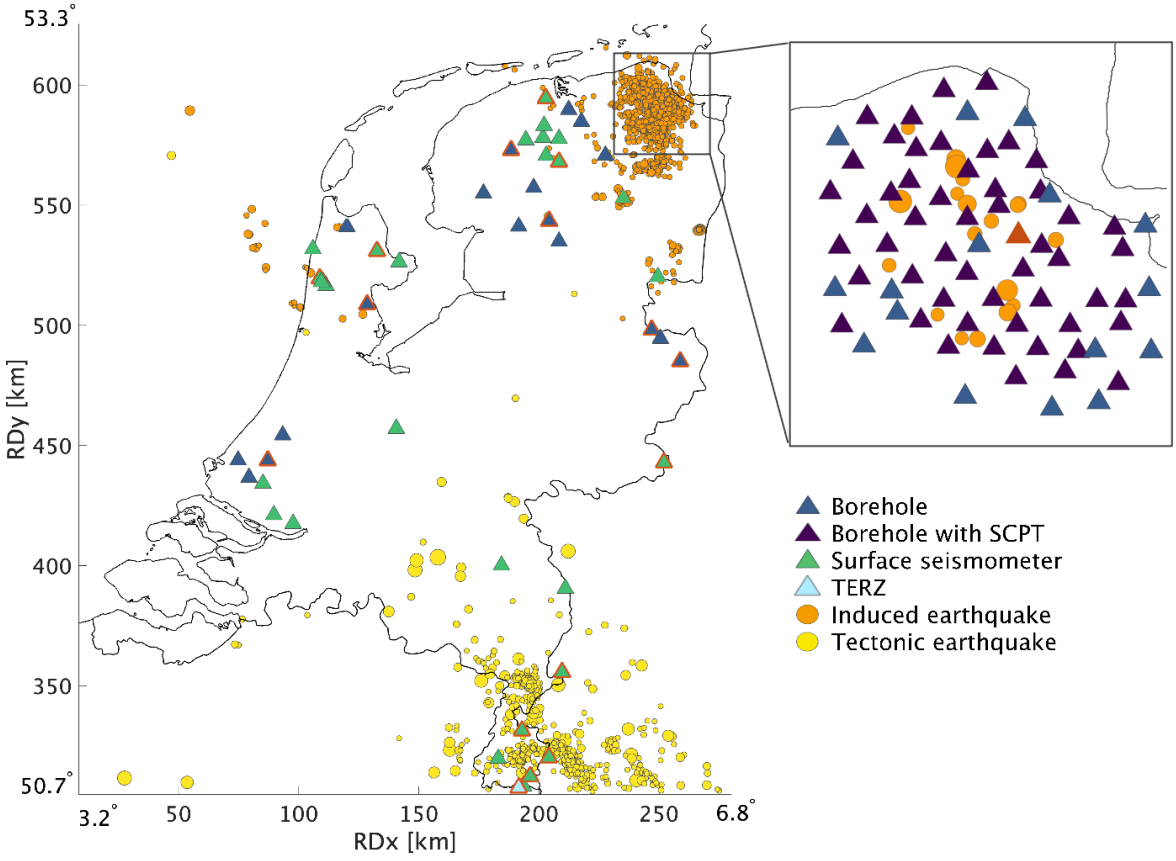

Figure 2: Map of the Netherlands depicting epicentres of all induced (Mw 0.5-3.6, orange) and tectonic (Mw 0.5-5.8, yellow) earthquakes from 1910-2020. The diameter of the circles indicates the relative earthquake magnitude. The triangles represent the surface location of the borehole stations (blue), borehole stations with SCPT measurement (purple) and single surface seismometers (green). The triangles with red outlines depict the locations of example HVSR curves presented in Figure 9. The inset in the north-east depicts the location of the Groningen borehole network (G-network). The 19 (Mw ≥2) induced earthquakes in this panel are used for the AF and ETF computations. Coordinates are shown within the Dutch National Triangulation Grid (Rijksdriehoekstelsel or RD) and lat/long coordinates are added in the corners for international referencing.

- The calculation of AFs need to be elaborated in mathematical terms and the signal processing aspects need to be explained better. The calculation of AFs for the event shown in Figure 3 can be presented as an example. The 1D geology and Vs profile at that location could also be presented to show if the AF could be explained/interpreted.

  It is a good suggestion to add the G24 velocity profile and corresponding lithology. Figure 3 is updated accordingly. The calculations of AFs are also explained in more detail in the updated manuscript. We decided not to show the equation since the procedure is easily conveyed in words.

- Which M>2 earthquakes have been used for the AF calculation – the induced or tectonic ones? How many earthquakes are there? What are their magnitude-distance distributions? Have they been selected based on good signal-to-noise ratio?

Thanks for pointing this out since this is important information to add. We used 19 M≥ 2 local induced earthquakes, added this number to the text. In Groningen, all earthquakes are induced (see Figure 2). We deliberately used the M≥2 earthquakes since lower magnitudes are not recorded across the entire network. By using 19 earthquakes with different magnitudes and distances, the magnitude-distance relationship (if present) is averaged out. Furthermore, we also included a signal-to-noise threshold to obtain reliable results.

- Why are the AFs calculated in such large frequency bands? Such results provide very little resolution for the interpretation of the amplification. Is there an estimate of the Vs of the sedimentary layer? Is it possible to verify if the fundamental resonance of amplification is captured within 1-5 Hz band?

  You have raised a good point here. The 1-10 Hz band captures the full range of possible resonance frequencies of most structures in the Netherlands and is the interval of interest for earthquake engineering purposes. By division into multiple spectra ordinates, we should design also multiple site-response zonation maps. This detailed revision is a good suggestion for future work.

  *Vs30 profiles are available from the SCPT's obtained next to the Groningen boreholes. From the relationship between Vs, and sediment thickness of the Holocene infill (f0=Vs/4*h) we can conclude that the resonance frequencies are mostly in the band of 1-5Hz. Van Ginkel et al. (2019) explains the relationship between the amplification and Holocene infill.*

- The authors mention that the high AFs in 1-5Hz band is due to fundamental resonances but they do not provide any evidence to support that.

  We refer to the paper Van Ginkel et al. (2019) to show that the fundamental resonances occur in this band.

- L205: Once again, which earthquakes have been used to compute the ETFs? The computation of the ETFs need to be elaborated with appropriate examples. This reviewer is not convinced by the interpretation of the ETFs. Do the ETF50 and ETF200 have similar amplitudes at all sites? Can it be supported by the geology of some example sites?

  The updated manuscript contains more detailed information on the earthquakes used. Additionally, a reference is added to the methodology of calculating transfer functions. Almost the entire Netherlands is covered with thick (> 200m) sediments. At 200 m the subsurface contains Pleistocene clastic sediments and only the top tens of meters comprise the (very) soft unconsolidated sediments. So almost everywhere the ETF200 resembles the ETF50. In Groningen, we observe at all sites with a computed ETF a relationship with the geology. It is a good point you raised; hence the updated manuscript includes a few lines on the relationship with the geology

- Figure 5: The visibility of this Figure is poor. It's difficult to verify the comparison among the curves. The X-axis is not graduated at all.

You have raised a good point here and accordingly the figure will be updated with larger fonts and a better distinction among the curves.

- L235: Which are the sites where HVSR, ETF and AF all are measured? Please show on the map. How many earthquakes (and their M-R distribution) are available for those sites? Figure 7 is not well explained and the Figure title is also unclear.What are the values plotted there? At which frequency?

  For the ETF and AF, we use 19 local earthquakes. These are all the $M \geq 2$ earthquakes recorded with the Groningen borehole network since it was deployed in 2015. In the new manuscript we will add a figure in Figure 2 (shown above) illustrating the earthquake epicentres and the boreholes used for the computations.

  The updated manuscript will contain an improved description and caption of Figure 7. In Figure 7, the y-axis are the AF values computed for the Groningen borehole network for 1-10 Hz, as presented in Section 4.2. Furthermore, subfigure labels are added to each panel in order to make references in the text. Additionally, the description of the axis labels is adjusted for more clarity.

- L 255: It seems that the Vs10, Vs20 and Vs30 values are taken from one set of sites and the Vs50 is taken from another. Is that so? Which of these sites correspond to the ones where AFs and ETFs are estimated? How far away the other sites are?

  The Vs10, Vs20 and Vs30 are values from the SCPT data obtained adjacent to 53 of the 68 borehole sites. Figure 2 displays the borehole locations where SCPTs have been taken. The Vs50 is computed based on records at the surface and 50 m deep seismometer for each borehole, as presented in Hofman et al., (2017), comprising the same sites as the SCPTs. So, all velocity-values used are at the borehole sites from which also the ETF, HVSR and AFs are computed.

- L 259: How are the depth and size of velocity contrast derived? It's not very clear from the description. Please provide mathematical formulation.

  Thanks for pointing out that this was missing. The velocity contrast is derived from the SCPT shear-wave velocity values. The contrast is computed by the division of the two different velocity values bounding each 1 m interval. This division is done for each 1 m interval over 30 m of SCPT records. The largest division value is defined as the velocity contrast (VC) and corresponding depth is the depth of the contrast (zVC).

- What is the rational of using the particular functional forms for fitting AF with Vs and VC? What are x1, x2, x3?

  Thanks for pointing this out, indeed this paragraph requires more clarity, accordingly in the new manuscript we change the x1, x2, x3 to a, b, c to avoid confusion with Cartesian coordinates. a, b and c are the three unknown

coefficients to be fitted. This line is rephrased for more clarity. The AF-Vs relationship exhibits an exponential fit, while the AF-VC is logarithmic.

- L 280: Where are these stations located? They could not be found anywhere in the article?

  Figure 2 is updated with the locations of the example HVSR (triangles with red outline)

- L 292: It's not evident to this reviewer that the borehole ETFs show most amplification within 50 m depth. Only one random example has been shown in Figure 5. The 50m, 200m depth values seem more like mere assumptions of the authors. In Figure 7, the fit between AF and Vs seems more or less similar for Vs10, Vs20, V30, Vs50. It rather seems that the functional relation could be slightly different in case of Vs10, Vs20 compared to Vs30, Vs50. As none of these results have been explained/supported throughout the paper by concrete geological and geophysical information, the summery and interpretation of the results seem very ambiguous.

  It is an important point you are raising here and accordingly we provide here an extra figure explaining the assumption that amplification largely occurs within the top 50m. Hence, Figure 3 below shows the ETF peak amplitudes for the ETF200, the ETF50 and the absolute difference (ETF200-ETF50) for the boreholes of the Groningen network. Overall, the small value for difference indicates that most amplification occurs in the top 50 m. Since the AF exhibits similar observations as discussed in van Ginkel et al. (2019) we decided not to include this in this manuscript.

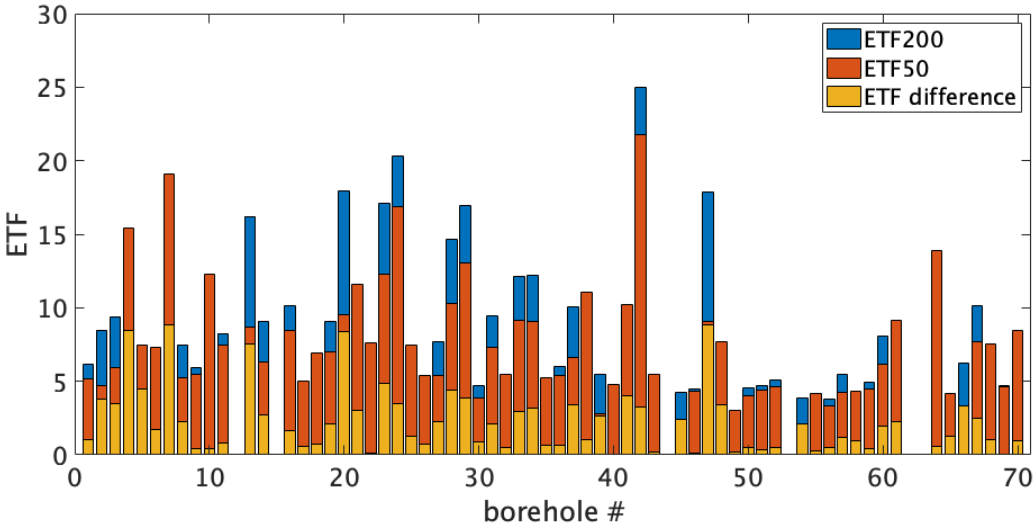

Figure 1: Bar plot illustrating the absolute difference (yellow) between the peak amplitude over a frequency band of 1-10 Hz ETF200 (blue) and the ETF50 (red) for each borehole in the Groningen network.. ETF

Secondly, you raised a good point here about missing the link between the Vs10-Vs20 fit and the geology. Accordingly, we added a few lines in section 4.5 about the relationship:

"In Groningen, the low-velocity and unconsolidated Holocene sediments have a thickness of 1-25 m and below these depths the velocities increase in the more compacted Pleistocene sediments. The reduced fitting quality of the Vs30 and Vs50 arises since the amplification develops mainly in the Holocene sediments (van Ginkel et al., 2019)."

Furthermore, Figure 8 is updated to show the link between the HVSR and corresponding sediment profile in order to add more information on the relationship between the seismological observation and the geology.

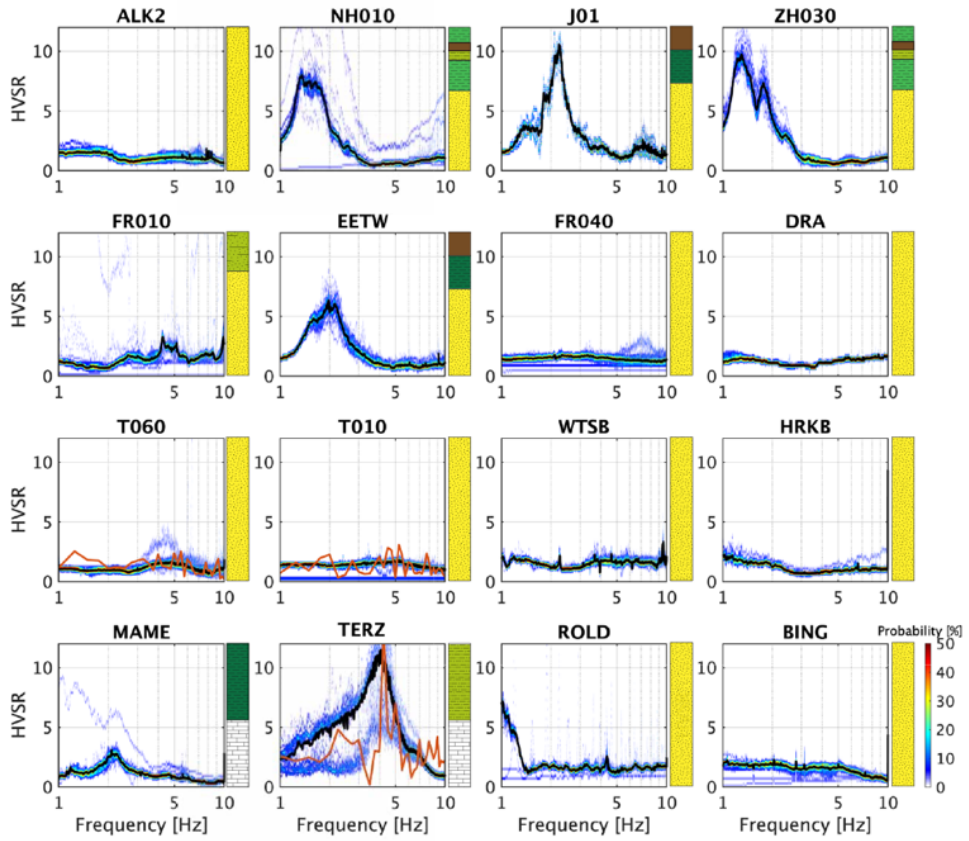

Figure 8: Each panel depicts a probability density function from ambient noise HVSR curves and sediment profile (Section 5) for 16 stations of the NL-network. The black line represents the mean HVSR and the red line in the panel of T06, T010 and TERZ represents the ETF calculated from 10 local earthquakes. The color bar in the lower right displays the HVSR probability range that is valid for all panels.

- This reviewer is also doubtful about the site classification approach in this article and, hence, about the entire zonation. Replicating the HVSR-AF correlation obtained from the limited Groningen area for the entire country seems a bit heavy-handed. In other studies (e.g., Perron et al.), HVSR has been shown as a complementary parameter for amplification prediction within an area where already some estimates of AF exist. The site-specific nature of amplification must be addressed in a zonation approach.

Thanks for pointing this out and as suggested in your review, we added more details of the methods and link to geology/geophysics to the updated manuscript. We believe the site classification approach presented is reasonable due to the following reasons:

1. *In the Netherlands, the shallow geology is laterally quite uniform in terms of recent depositional history (see geological map, Figure 1). Therefore, the correlations obtained from the Groningen area are quite representative for the majority of the country. This area contains the most recent Holocene unconsolidated sediments, as well as the Pleistocene sand that cover a large part of the country. Hence, a large part of the typical NL sites is covered within the Groningen region.*
2. *For locations with a deviating Holocene or Pleistocene top 50 m, like the coastal dunes, we analyze the HVSR curves estimated from ambient vibrations recorded at seismometers throughout the country and link it to the geology at that site. This is to expand the sediment classification in order to address the site-specific nature of amplification.*
3. *We observe strong similarities in terms of curve characteristics and subsurface geology between the HVSR estimations throughout the country and the HVSR characteristics in Groningen. This confirms that amplification in the top 50 m sediment layer develops consistently throughout the country.*
4. *Each HVSR curve is linked to the sediment profile classification. This is justified with more details in Figure 4 of this response.*
5. *Due to the uniform sedimentation of the clastics, the AF-HVSR correlation derived from Groningen seems a reasonable first approach for country-wide AFs. With more data available on AFs at multiple locations, the AF-HVSR relationship can be optimized by using the approach described in e.g. Cultrera et al. (2014), Perron et al. (2018) and Panzera et al. (2021).*
6. *In order to correct for the locations with deviating and shallow 'bedrock' (<100 m) conditions, we designed class V. This setting is absent in Groningen so we are not able to define AFs here. This class needs further investigation for site-response and AF estimations and this is discussed in the manuscript.*
7. *We are aware that our approach comes with uncertainties and we address the AF uncertainty in Section 6.3.*
8. *Lastly, this manuscript presents a first approach for the zonation, when more data becomes available, the map can be updated accordingly. But for a first site-response estimation at locations with limited data available, we believe our approach is reasonable.*

- This reviewer suggests the authors to highlight the geology more and verify/interpret/constrain the results in terms of the geology of the measurement sites. It's important to explain the effects of the subsurface structure/geology on the amplification rather than drawing purely statistical functional correlations.

Thanks for pointing this out and accordingly we have added more details on the geology and the relationship with the seismological and geophysical observations (see the previous points). Also, we refer to van Ginkel et al. (2019), which reference describes in detail the relationship between geology and amplification in Groningen.

Your editorial remarks will be incorporated in the new manuscript. Furthermore, the manuscript is carefully read to address writing imperfections. We hope we cover your comments and are willing to respond to any further questions and suggestions you may have.

Sincerely,

Janneke van Ginkel, Elmer Ruigrok, Jan Stafleu and Rien Herber

References

Cultrera, G., De Rubeis, V., Theodoulidis, N., Cadet, H., & Bard, P.-Y. Statistical correlation of earthquake and ambient noise spectral ratios.Bulletin of earthquake engineering,12(4), 1493–1514, 2014.

Hofman, L., Ruigrok, E., Dost, B., and Paulssen, H.: A shallow seismic velocity model for the Groningen area in the Netherlands, Journal ofGeophysical Research: Solid Earth, 122, 8035–8050, 2017.

Kruiver, P. P., van Dedem, E., Romijn, R., de Lange, G., Korff, M., Stafleu, J., Gunnink, J. L., Rodriguez-Marek, A., Bommer, J. J., van Elk,J., et al.: An integrated shear-wave velocity model for the Groningen gas field, the Netherlands, Bulletin of Earthquake Engineering, pp.1–26, doi: 10.1007/s10518-017-0105-y, 2017a

Panzera, F., Bergamo, P., and Fäh, D.: Canonical Correlation Analysis Based on Site-Response Proxies to Predict Site-Specific AmplificationFunctions in Switzerland, Bulletin of the Seismological Society of America, 2021.

Perron, V., Gélis, C., Froment, B., Hollender, F., Bard, P.-Y., Cultrera, G., and Cushing, E. M.: Can broad-band earthquake site responses be predicted by the ambient noise spectral ratio? Insight from observations at two sedimentary basins, Geophysical Journal International, 215, 1442–1454, 2018.

Poggi, V., Edwards, B., and Fäh, D.: Derivation of a reference shear-wave velocity model from empirical site amplification, Bulletin of the705Seismological Society of America, 101, 258–274, 2011.

van Ginkel, J., Ruigrok, E., and Herber, R.: Assessing soil amplifications in Groningen, the Netherlands, First Break, 37, 33–38, 2019.

Development of a country-wide seismic site-response zonation map for the Netherlands

Janneke van Ginkel[1,2], Elmer Ruigrok[2,3], Jan Stafleu[4], and Rien Herber[1]

[1]Energy and Sustainability Research Institute Groningen, University of Groningen, Nijenborgh 6, 9747 AG Groningen, the Netherlands.
[2]R&D Seismology and Acoustics, Royal Netherlands Meteorological Institute, Utrechtseweg 297, 3731 GA De Bilt, the Netherlands.
[3]Department of Earth Sciences, Utrecht University, Princetonlaan 8a, 3584 CB Utrecht, the Netherlands
[4]TNO - Geological Survey of the Netherlands, Princetonlaan 6, 3584 CB Utrecht, the Netherlands

Correspondence: Janneke van Ginkel (j.a.van.ginkel@rug.nl, ORCID-iD 0000-0001-7601-5119)

Abstract.

Earthquake site-response is an essential part of seismic hazard assessment, especially in densely populated areas. The shallow geology of the Netherlands consists of a very heterogeneous soft sediment cover, which has a strong effect on ~~seismic wave propagation and in particular on~~ the amplitude of ground shaking~~, resulting in significant damage on structures despite the fact that the events are of small magnitude~~. Even though ~~it~~ the Netherlands is a low-to-moderate seismicity area, the seismic risk cannot be neglected, in particular, because shallow induced earthquakes occur. The aim of this study is to establish a ~~nationwide~~ nation-wide site-response zonation by ~~using the lithostratigraphy~~combining 3D lithostratigraphic models, earthquake- and ambient vibration recordings.

~~In the~~ As a first step, we constrain the parameters (velocity contrast and shear-wave velocity) that are indicative of ground-motion amplification in the Groningen area. For this, we ~~combine~~ compare ambient vibration and earthquake recordings using resp. the horizontal-to-vertical spectral ratio method (HVSR), borehole empirical transfer functions (ETFs) and amplification factors (AFs). This enables us to define an empirical relationship between ~~measured earthquake amplification from~~ the amplification measured from earthquakes by using the ETF and AF, and ~~amplification estimated with the HVSR derived from the ambient seismic field. Therewith~~the amplification estimated from ambient vibrations by using the HVSR. With this, we show that the HVSR can be used as a first proxy for ~~amplification.~~

site-response. Subsequently, HVSR curves throughout the Netherlands are estimated. The ~~resulting peak amplitudes~~ HVSR amplitude characteristics largely coincide with the in-situ lithostratigraphic sequences and the presence of a strong velocity contrast in the near-surface. Next, sediment profiles representing the Dutch shallow subsurface are categorized into five classes, where each class is representing a level of expected amplification. The mean amplification for each class, and its variability, is quantified using 66 sites with measured earthquake amplification (ETF and AF) and 115 sites with HVSR curves.

The site-response (amplification) zonation map for the Netherlands is designed by transforming ~~published~~ geological 3D grid cell models into the five classes and an AF is assigned to most of the classes. This ~~presented~~ this site-response assessment~~on~~

~~a national~~ , presented on a nation-wide scale is important for a first identification of regions with increased seismic hazard potential, for example at locations with mining or geothermal energy activities.

1 Introduction

~~Local near-surface~~ Site-response estimation is a key parameter for seismic hazard assessment and risk mitigation, since local lithostratigraphic conditions can strongly influence the level of ~~amplification of seismic ground-motion~~ ground motion amplification during an earthquake (e.g. ~~Bard et al. (1988); Bard (1998); Bonnefoy-Claudet et al. (2006b, 2009); Borcherdt (1970); Bradley~~ Especially near-surface low-velocity sediments overlying stiffer bedrock modify earthquake ground-motions in terms of ~~amplitudes~~ amplitude and frequency content, ~~the so-called seismic site-response.~~

~~Site conditions may be retrieved from available global datasets and the ground-shaking estimation is based on ground-motion prediction equations (Akkar et al., 2014; Bindi et al., 2014).~~ as for instance observed after the Mexico City earthquake in 1985 (Bard et al., 1988) as well as more recent ones (e.g. L'Aquila, Italy, 2009; Tokyo, Japan, 2011; Darfield, New Zealand 2012). Site-response ~~estimation~~ estimations require detailed geological and ~~geo-technical~~ geotechnical information of the subsurface~~, which~~ . This can be retrieved from in-situ investigations, however, this is a costly procedure. Because of the time and costs involved, there is a lack of site-response investigations covering large areas, while the availability of detailed and uniform ground-motion amplification maps is fundamental for preliminary estimates of damage on buildings (e.g. Falcone et al. (2021); Gallipoli et al. (2020); Bonnefoy-Claudet et al. (2009); Weatherill et al. (2020)). ~~In the present work, a procedure is developed to obtain an amplification map for the Netherlands which is both detailed and spatially extensive. Key ingredients are a detailed lithostratigraphic model and a plurality of seismic recordings.~~

~~Overall, the shallow geology of the Netherlands consists of a very heterogeneous soft sediment cover, which has a strong effect on seismic wave propagation and in particular on the amplitude of ground shaking.~~ Empirical seismic site-response is widely investigated by the use of microtremor horizontal-to-vertical spectral ratios (HVSR, e.g. Fäh et al. (2001); Lachetl and Bard (1994); The HVSR is obtained by taking the ratio between the Fourier amplitude spectra of the horizontal and the vertical components of a seismic recording. When a shallow velocity contrast is present, the peak in the HVSR curve is closely related to the shear-wave resonance frequency for that site. However, the HVSR peak amplitude cannot be treated as the actual site amplification factor, but serves as a qualitative estimate (Field and Jacob, 1995; Lachetl and Bard, 1994; Lermo and Chavez-Garcia, 1993).

The Netherlands experiences tectonically related seismic activity in the southern part of the country, with magnitudes up to 5.8 measured so far (Camelbeeck and Van Eck, 1994; Houtgast and Van Balen, 2000; Paulssen et al., 1992). Additionally, gas extraction in the northern part of the Netherlands is regularly causing shallow (3 km), low magnitude ($Mw \leq 3.6$ thus far) induced earthquakes (Dost et al., 2017). Over the last decades, an increasing number of these induced seismic events stimulated the research on earthquake site-response in the Netherlands.

Various studies (van Ginkel et al., 2019; Kruiver et al., 2017a, b; Bommer et al., 2017; Noorlandt et al., 2018) undertaken in the Groningen area ~~concluded that unconsolidated sediments were~~ (north-eastern part of the Netherlands) concluded that the heterogeneous unconsolidated sediments are responsible for significant amplification of seismic waves over a range of frequencies pertinent to engineering interest. Although the local earthquake magnitudes are relatively small, the damage ~~on~~ to the houses can be significant. Hence multiple studies (e.g. Rodriguez-Marek et al. (2017); Bommer et al. (2017); Kruiver et al. (2017a); Noorlandt et al. (2018)) were performed on ground-motion modeling including the site amplification factor for the Groningen region~~, which~~ .

Groningen forms an excellent study area due to the presence of the permanently operating borehole seismic network (G-network). ~~Here, earthquake recordings and ambient noise measurements, together with detailed subsurface information form an elaborate dataset to study wave propagation in the shallow subsurface (van Ginkel et al., 2019).~~ Local earthquake recordings ~~in boreholes over a range of depth levels~~ over the Groningen borehole show that the largest amplification ~~occurs~~ develops in the top 50 meters of the sedimentary cover (van Ginkel et al., 2019), although the entire sediment layer has a thickness of around 800 m in this region. Furthermore, van Ginkel et al. (2019) showed existence of a the correlation between the spatial distribution of microtremor horizontal-to vertical spectral ratio (HVSR) peak amplitudes and the measured earthquake amplification. This observation is in accordance with those of e.g. ~~Perron et al. (2018) and Pilz et al. (2009)~~ Pilz et al. (2009); Perron et al. (2018); Panzera et al. (20 show a comparison of site-response techniques using earthquake data and ambient seismic noise analysis. ~~In Our study, we first select the Groningen borehole network where a detailed information on subsurface lithology, numerous earthquake ground-motion recordings as well as ambient seismic noise recordings are available. From this we extract empirical relationships between seismic wave amplification and different lithostratigraphic conditions, building upon the proxies defined in van Ginkel et al. (2019)~~

The ~~microtremor HVSR technique is widely used (Fäh et al., 2001; Lachetl and Bard, 1994; Bonnefoy-Claudet et al., 2006a; Albarello a proxy for site-response and seismic zonation studies and was first proposed by Nogoshi and Igarashi (1970) and widespread by Nakamura (1989, 2019). The HVSR is obtained by taking the ratio between the Fourier amplitude spectra of the horizontal and the vertical components of ambient noise vibrations recorded at a single station. The HVSR of the seismic noise presents peaks which are related to the resonances of shear-waves in the top sediment layer. The HVSR peak amplitude cannot be treated as the actual site amplification factor, but can serve as a qualitative estimate (Field and Jacob, 1995; Lachetl and Bard, 1994; Lermo and Chavez-G In this study we focus on the second peak ($\geq$ 1 Hz) in the HVSR curve which represents the shallow interface of soft sediments on top of more consolidated sediments instead of the resonance of the complete sediment layer as discussed in van Ginkel et al. (2020). This second amplification peak has shown to play a more important role for seismic site-response at frequencies relevant to engineering interest. The HVSR method is applied on the Netherlands seismic network to assess site-response based on ambient vibrations.~~

~~The Eurocode 8 seismic design of buildings (CEN et al., 2004) describes the effect of characteristics on soil behaviour during an earthquake and the seismic response of buildings. In order to estimate the risk of enhanced site-response, five soil types are provided based on shear-wave velocities and stratigraphic profiles. Soil-type E in Eurocode 8 is essentially characterised by a sharp contrast of a soft layer overlying a stiffer one. However, in our opinion, this single classification for soft sediments is~~

~~rather limited, especially concerning the wide variety of lithostratigraphic conditions throughout the Netherlands. Therefore,~~ ~~we present an alternative, or extended, classification for ground characteristics designed to specify the large heterogeneity in site conditions that exists within Eurocode 8 ground-type E.~~

~~The~~ aim of this work is to design a site-response zonation map for the Netherlands, which is both detailed and spatially extensive. Rather than using ground-motion prediction equations with generic site amplification factors conditioned on Vs_{30}, ~~a national~~ we propose a novel approach for the development of a nation-wide zonation of amplification factors~~is developed~~. To this end, we combine multiple seismological records, geophysical data and detailed 3D lithostratigraphic models in order to estimate and interpret site-response. We first select the Groningen ~~region to test~~ borehole network where detailed information on subsurface lithology, numerous earthquake ground-motion recordings as well as ambient seismic noise recordings are available since their deployment in 2015. From this, we extract empirical relationships between ~~measured earthquake amplification and site-response derived from the HVSR estimations.~~ seismic wave amplification and different lithostratigraphic conditions, building upon the proxies defined in van Ginkel et al. (2019).

Next, the ambient vibration measurements of the seismic network across the Netherlands are used, necessary to calibrate the amplification (via HVSR) with the local lithostratigraphic conditions. ~~Combining~~ By combining the detailed 3D geological subrsurface models GeoTOP (Stafleu et al., 2011, 2021) and NL3D (Van der Meulen et al., 2013), with a derived classification scheme, a zonation map for the Netherlands is constructed.

The presented site-response zonation map for the Netherlands is especially designed for seismically quiet regions where tectonic seismicity is absent, but with a potential risk of induced seismicity, for example due to mining or geothermal energy activity (Majer et al., 2007; Mena et al., 2013; Mignan et al., 2015). As a result, this map can be implemented in seismic hazard analysis.

2 Geological setting and regional seismicity

The Netherlands is positioned at the southeastern ~~rim of the North Sea sedimentary~~ margin of the Cenozoic North Sea basin. The ~~sediments at the surface are almost entirely Quaternary with the thickest succession (600~~onshore basin infill is characterized by Paleogene, Neogene and Quaternary sediments reaching a maximum thickness of ~1800 m~~) occurring in the northwest (Zagwijn, 1989; Rondeel et al., 1996; De Gans, 2007). Neogene and older sediments are only exposed in the farthermost east and south of the country, where the edges of the North Sea Basin were uplifted and eroded~~. Minimum onshore thicknesses are reached along the basin flanks in the eastern and southern Netherlands and locally at uplifted blocks like the Peel Block. The main tectonic feature of the country is the Roer Valley Graben, bounded by the Peel Boundary Fault in the northeast and the Rijen, Veldhoven and Feldbiss Faults in the south and southwest (Figure 1).

The ~~surface geology~~ Paleogene and Neogene sediments are dominated by marine clays and sands that were primarily deposited in shallow marine environments. The Quaternary sediments, reaching a maximum onshore thickness of ~600 m, reflect a transition from shallow marine to fluvio-deltaic and fluvial depositional environments in the early Quaternary to a complex alternation of shallow marine, estuarine and fluvial sediments in the younger periods (Zagwijn, 1989; Rondeel et al., 1996; De Gan

Imprints of glacial conditions are recorded in the upper part of the basin fill by among others, deep erosive structures (subglacial valleys, tongue basins) and glacial till (Van den Berg and Beets, 1987).

2.1 Surface geology

The surface geology (Figure 1) is mainly characterized by a Holocene coastal barrier and coastal plain in the west and north, and an interior zone with Pleistocene deposits cut by a Holocene fluvial system ~~(Rondeel et al., 1996)~~(Rondeel et al., 1996; Beets and van der S
The coastal barrier consists of sandy ~~beach~~ shoreface and dune deposits and is up to 10 km wide. It is intersected in the south by the estuary of the ~~rivers~~ Rhine, Meuse and Scheldt, and in the north by the tidal inlets of the Wadden Sea. The coastal plain ~~mainly consists~~ is formed by mainly of marine clay as well as peat. Although much of the peat has disappeared because of mining and drainage, thick sequences of peat ($>$ 6 m) still occur. The Holocene fluvial deposits of the rivers Rhine and Meuse are characterized by a complex of sandy channel belt systems embedded in flood basin clays (Gouw and Erkens, 2007). The fluvial channel belts pass downstream into sandy tidal channel systems in the coastal plain (Hijma et al., 2009).

The Pleistocene interior of the country mainly consists ~~of~~ glacial, eolian and fluvial deposits (Rondeel et al., 1996; Van den Berg and Bee
Glacial deposits include ~~coarse-grained~~ coarse grained meltwater sands and tills. Ice-pushed ridges, with heights up to 100 m, occur in the middle and east of the country. Eolian deposits mainly consist of cover sands ~~,~~and are locally made up by drift sand and inland dunes. In the south and east of the country, sandy channel and clayey flood basin deposits of small rivers occur.

Neogene and older deposits are only exposed in the eastern- and southernmost areas of the country. In the east, these sediments include unconsolidated Paleogene formations as well as Mesozoic limestones, sandstones ~~an~~ and shales. In the south, the older deposits comprise unconsolidated Neogene and Paleogene sands and clays, as well as Cretaceous limestones (chalk), sandstones and shales, and Carboniferous sandstones and shales.

2.2 Regional seismicity

The Netherlands experiences ~~two types of seismicity; firstly, earthquakes in the south-east are caused by deep tectonic processes and secondly, induced seismicity~~ tectonically related earthquake activity in the south east and induced earthquakes occur in the north at shallow depths ~~triggered by~~ due to exploitation of gas fields~~(Figure 2)~~. Tectonic seismicity occurs mainly in the Roer Valley Graben (yellow circles, Figure 2) which is part of a larger basin and range system in Western Europe, the Rhine Graben Rift System. At the beginning of the Quaternary, the ~~rate of subsidence~~ subsidence rate in the Roer Valley Graben ~~has significantly increased~~ did increase significantly (Geluk et al., 1995; Houtgast and Van Balen, 2000) and the rift system still shows active extension (Hinzen et al., 2020). The largest earthquake recorded (Mw=5.8) in the Netherlands was in Roermond in 1992, due to extensional activity along the Peel Boundary Fault (Paulssen et al., 1992). Gariel et al. (1995) quantified the near-surface amplification based on spectral ratios of aftershocks from the 1992 earthquake in Roermond. They observed great variety in ground-motion amplitudes over different stations which is ~~very likely a~~ the site effect of shallow sedimentary deposits.

Most induced earthquakes in the Netherlands (orange circles, Figure 2) have their epicentre in the Groningen region due to production of the gas field. Here, reservoir compaction due to pressure depletion has reactivated the existing normal fault

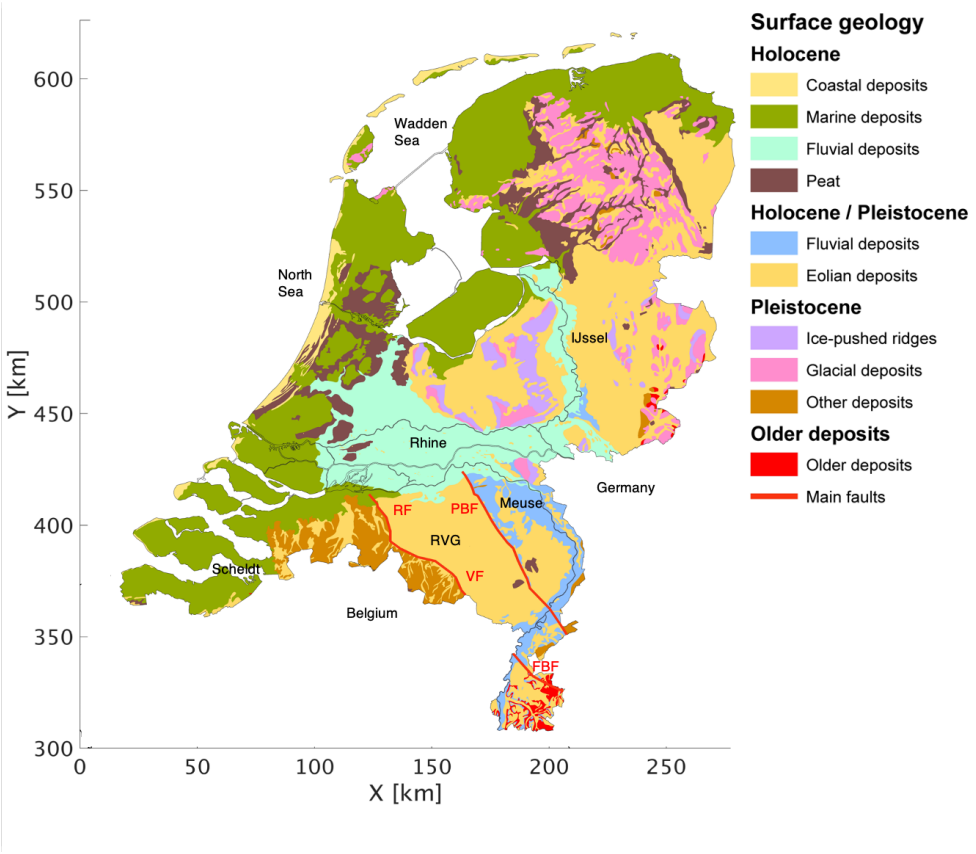

Figure 1. ~~Geological~~ Surface geological map of the Netherlands. Older deposits comprise unconsolidated Neogene and Paleogene deposits as well as Mesozoic and Carboniferous limestones, sandstones and shales. Modified after Schokker (2010). RF = Rijen Fault, VF = Veldhoven Fault, PBF = Peel Boundary Fault, FBF = Feldbiss Fault, RVG = Roer Valley Graben.

system that traverses the reservoir layer throughout the whole field. (Buijze et al. (2017); Bourne et al. (2014)). Even though the magnitudes are relatively low (van Thienen-Visser and Breunese, 2015), the damage ~~on~~ to buildings in the area is substantial due to shallow hypocenters and amplification on the soft near-surface soils (Bommer et al., 2017; Kruiver et al., 2017a).

3 Data set

For this study, we use the seismic network of the Royal Netherlands Meteorological Institute (KNMI, 1993)~~across the Netherlands is used~~, consisting of borehole and surface seismometers distributed over the Netherlands (Figure 2). The ~~blue and purple triangles represent~~ network includes 88 locations ~~of the borehole network~~ with vertical borehole arrays where each station is equipped with three-component, 4.5 Hz seismometers at 50m depth intervals (50, 100, 150, 200 m) and an accelerometer at the

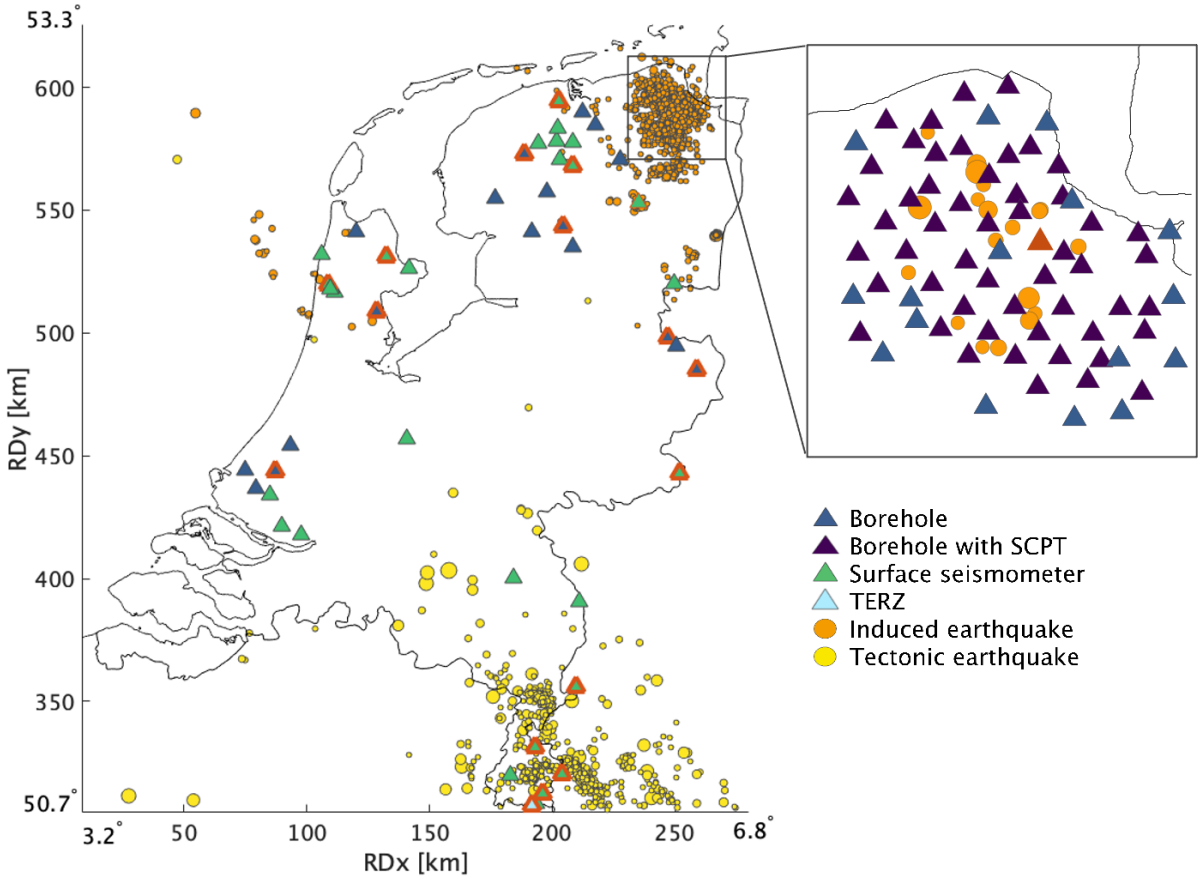

Figure 2. Map of the Netherlands depicting epicentres of all induced (Mw 0.5-3.6, orange) and tectonic (Mw 0.5-5.8, yellow) earthquakes from 1910-2020. The diameter of the circles indicates the relative earthquake magnitude. The triangles represent the surface location of the borehole stations (blue), borehole stations with SCPT measurement (purple) and single surface seismometers (green). The triangles with red outlines depict the locations of example HVSR curves presented in Figure 8. The inset in the north-east depicts the location of the Groningen borehole network (G-network). Here, the red triangle depicts the location of borehole G24. The 19 ($Mw \geq 2$) induced earthquakes in this panel are used for the AF and ETF computations. Coordinates are shown within the Dutch National Triangulation Grid (Rijksdriehoekstelsel or RD) and lat/~~lon~~ long coordinates are added in the corners for international referencing.

surface. The ~~purple triangles indicate boreholes where an S-wave velocity profile is available from a Seismic Cone Penetration Test (SCPT). The~~ southernmost station is at Terziet (TERZ~~, light blue triangle in Figure 2~~). This station consists of a borehole seismometer at 250 m depth and a surface seismometer. ~~The green~~ In Groningen, multiple boreholes have Seismic Cone Penetration Tests (SCPT) taken directly adjacent to the borehole. The remaining triangles represent 29 locations of single surface seismometers (accelerometers and broad bands). All seismometers have three components and are continuously recording

the ambient seismic field and, when present, local ~~seismic events. The~~ earthquakes. In Section 4 we use 19 local earthquakes of M≥2, recorded in the Groningen borehole network between 05-2015 and 05-2019. All data is available through the KNMI data portal (http://rdsa.knmi.nl/network/NL/).

In the construction of the site-response map we have made extensive use of the detailed 3D geological subsurface models GeoTOP and NL3D. Both models are developed and maintained by TNO – Geological Survey of the Netherlands (Van der Meulen et al., 2013). GeoTOP schematizes the shallow subsurface of the Netherlands in a regular grid of rectangular blocks (voxels, tiles or 3D grid cells), each measuring 100 by 100 by 0.5 m (x ,y, z) up to a depth of 50 m below ordnance datum (Stafleu et al., 2011, 2021). Each voxel contains multiple properties that describe the geometry of lithostratigraphic units (formations, members and beds), the spatial variation of lithology and sand grain-size within these units as well as measures of model uncertainty. GeoTOP is publicly available from the TNO's web portal: https://www.dinoloket.nl/en/subsurface-models To date, the GeoTOP model covers about 70% of the country (including inland waters such as the Wadden Sea). For the missing areas we have used the lower-resolution voxel model NL3D, which is available for the entire country (Van der Meulen et al., 2013). NL3D models lithology and sand grain-size classes within the geological units of the layer-based subsurface model DGM (Gunnink et al., 2013) in voxels measuring 250 by 250 by 1 m (x ,y, z) up to a depth of 50 m below ordnance datum. To determine the depth of bed rock in the shallow subsurface, we consulted the layer-based subsurface models DGM and DGM-deep. These models are also available from the web portal mentioned above. More details on the models GeoTOP and NL3D are given in Appendix B.

4 Empirical relationships from the Groningen borehole network

The ~~extensive data set recorded with the~~ dense Groningen borehole network (G-network) provides the opportunity to derive empirical relationships between measured amplification in the time and frequency domain, estimated amplification from ~~the ambient noise field~~ ambient vibrations and the local lithostratigraphic conditions. ~~Ground-motion amplification is linked to specific subsurface conditions, hence this section elaborates on which of the subsurface parameters mainly influence the level of amplification: the shear-wave velocity and the velocity contrast.~~ First, we ~~define amplification and~~ present results of three different methods to assess ~~it~~amplification. Next, we compare ~~the~~ subsurface parameters with the measured amplification ~~to be able to~~ in order to evaluate which parameters are most critical.

4.1 Definition of amplification

The majority of site-response studies define the level of soft sediment amplification with respect to the surface seismic response of a nearby outcropping hard rock. ~~Due to the fact that in the Netherlands~~In the Netherlands, no representative seismic response ~~on~~ of outcropping bedrock is available~~, we decided to set the reference 'seismological bedrock' at a predefined depth of~~ . As an alternative, we define reference conditions as found in Groningen at 200 m ~~. This depth and corresponding average~~ depth, where we have many seismic recordings. These same reference conditions can be found at this depth over most locations in the Netherlands, though it can be sometimes deeper or shallower than 200 m. The corresponding elastic properties (shear-

wave velocity ~~forms~~ and density) form the basis from which the ~~site-response and corresponding amplification factors (AFs) are estimated in the next sections. With respect to a reference horizon at depth, waves are also amplified at~~ ground motion amplification effect of any site with respect to the reference can be predicted. This approach is akin the reference velocity profile that is used in Switzerland (Poggi et al., 2011).

For a recording at the Earth's surface~~due to~~, simultaneously the up- and down-going waves are recorded, which leads to an amplitude doubling. This is called the free-surface effect. ~~With~~ If the amplification is defined with respect to a surface (hard-rock~~reference site at the Earth's surface, however, there would be no additional~~) site, both the site of investigation and the reference site experience the same free-surface effect and there is no need to remove it in order to isolate the relative amplification. We have a reference site at depth, where no free-surface effect ~~. For this reason, we keep~~ takes place. Hence, we need to remove the free-surface effect ~~out of the AF definition~~first from the surface recording before isolating the relative amplification.

The ~~Groningen borehole network (~~G-network ~~)~~ forms a representative resource for the definition of the reference ~~rock parametersat~~ horizon parameters. Hofman et al. (2017) and (Kruiver et al., 2017a) determined shear-wave velocities at all borehole seismometers levels in Groningen. From their velocities found at 200 m depth~~. Here, the subsurface is composed of Pleistocene-and Pliocene sediments~~, the average is taken, resulting in a reference shear-wave velocity of 500 m/s. At this depth, the sediment density is on average 2.0 kg/m^3. At 200 m depth, 95% of the Dutch subsurface is composed of ~~these sedimentsat this depth~~laterally extensive Pleistocene-and Pliocene sediments, hence the estimated site-response and corresponding amplification factors can be applied on a large part of the country. The remaining 5% ~~consist~~ consists of shallow (<100 m) Triassic, Cretaceous and locally Carboniferous bedrock, and therefore these locations need to be evaluated separately. ~~Hofman et al. (2017) and (Kruiver et al., 2017a) determined shear-wave velocities at borehole stations in Groningen. From the velocities found at 200 m depth, the average is taken, resulting in a reference shear-wave velocity of 500 m/s. At this depth, the density is on average 2.0 kg/m^3.~~

~~Many studies (e.g., Bommer et al., 2017; Rodriguez-Marek et al., 2017; Borcherdt, 1994) model site-response amplification factors (AF) for different periods of spectral-accelerations. This study however is empirically driven, taking advantage of the large amount of high-quality data available. Particle velocity based AFs are derived between the site and the reference horizon at 200 m, in a frequency range of 1-10 Hz. In the next section we elaborate on the frequency band chosen.~~

4.1.1 Frequency bandwidth

Data processing is applied on a frequency bandpass filter for 1-10 Hz, covering the periods of interest from an earthquake engineering point of view. Moreover, for these frequencies, the used instrumentation (broadband seismometers, accelerometers and geophones) have high sensitivity for ground-motion.

Since ~~the majority of~~ most of the amplification is occurring in the top sedimentary layer (van Ginkel et al., 2019), the corresponding resonance frequencies are covered in the used frequency filter as well. Above 10 Hz~~the amplitude increases~~, the amplitude increase due to soil softening and resonance is counteracted by an-elastic attenuation and 3D scattering. Furthermore, what exactly happens above 10 Hz is of little interest since ~~the most energy~~ most of the local ~~earthquakes~~ earthquake energy

is contained in the frequency band between 1 and 10 Hz. This is illustrated in Figure 3, which presents the particle-velocity Fourier Amplitude Spectrum of ~~an event recorded on the radial component~~ a local earthquake recorded in borehole G24. The location of this borehole is presented as red triangle in Figure 2.

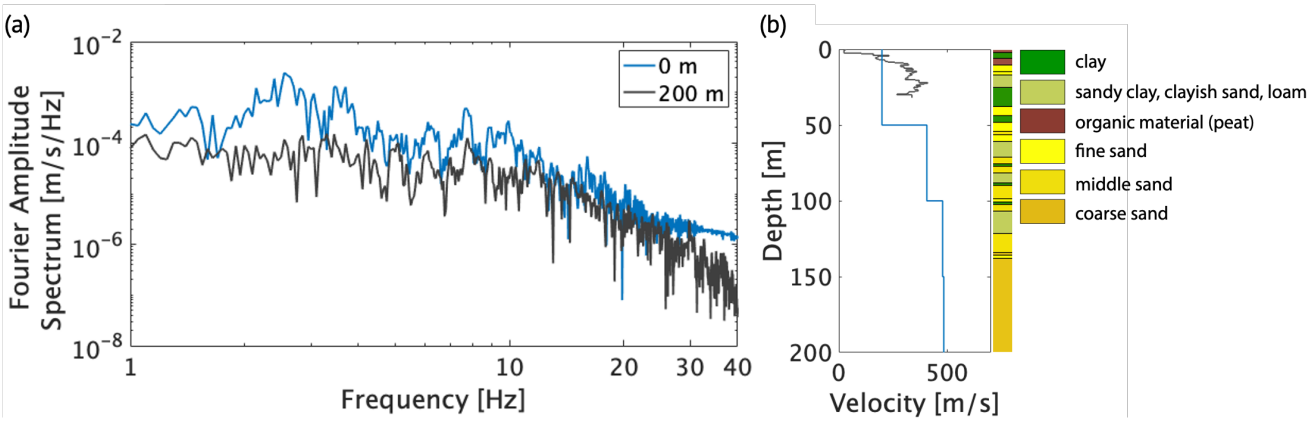

Figure 3. a) Particle velocity Fourier Amplitude Spectrum measured on the radial component for the 200 m (gray) and surface seismometer (blue) for borehole G24 for a ~~time window of~~ 20 s ~~after a local~~ time window of the 08-01-2018 Zeerijp M3.4 earthquake. Borehole G24 has an epicentral distance of 10 km. b) Shear-wave velocity profile for G24 with in blue the interval velocities from Hofman et al. (2017), and the shear-wave velocity from the adjacent SCPT over the top 30 m (black line). The corresponding lithological profile is derived from GeoTop (www.dinoloket.nl/subsurface-models, last access 15-10-2021).

4.2 Amplification Factors

~~In this study we compute amplification factors (AF) in the time domain~~ We compute an overall amplification factor from the G-network earthquake recordings ~~. We compute the AF for each borehole site~~ by taking the ratio of the maximum amplitudes recorded at the surface and the 200 m deep seismometer, following the procedure described in van Ginkel et al. (2019). This ratio is taken for both the radial (R) and transverse (T) component and the results are averaged. The amplitude at the surface ~~was~~ is divided by a factor of 2 in order to remove the effect of ~~free surface amplification.~~ the up-and down going waves recorded at the same time. Earthquake records are processed in the time domain for a 20 s time window and frequency band of 1-10 Hz. Next, the AF per borehole is obtained by repeating the above procedure for ~~all available M>~~19 available M≥2.0 ~~events~~ local induced earthquakes and subsequently averaging the values.

~~We decided to adapt the frequency band and seismometer depth to obtain an AF that is more representative for use on a national scale than the AF used in the region of Groningen. Hence in this paper, the AF is calculated between the seismometers at surface and at 200 m depth, for a frequency band of 1-10 Hz. The AF is~~ It is determined in the time domain and therewith ~~it~~ provides an average amplification over the applied frequency band. ~~To support the choice for using a single~~

Many studies (e.g., Bommer et al., 2017; Rodriguez-Marek et al., 2017; Borcherdt, 1994) model site-response amplification factors (AF) for different periods of spectral-accelerations, which is tailoring to engineering structures with different resonance

frequencies. In this study we aim to provide an average amplification level in a broad frequency band. The choice for the specific AF frequency band ~~, we calculate~~ was supported by evaluating amplification over a range of frequency bands. Figure 4 shows the AFs over the Groningen network for several ~~frequency bands(Figure 4). AF values~~ bands. AF-values are highest in the band 1-5 Hz ~~. This is related~~ due to the strong resonances ~~in this band~~of the Holocene infill (van Ginkel et al., 2019). In the 1-10 Hz band the AFs are lower~~. In the 5-10 Hz band still~~ , but contains considerable earthquake amplitudes ~~are present~~ (Figure 3)~~, whereas less amplification takes place than in the 1-5 Hz band~~. When the frequency band is extended beyond 10 Hz ~~,~~ (Figure 4c, d), the AF-values are not changing ~~much anymore, hence, a representative AF is obtained by limiting the band at 10~~significantly. We decided to pick the frequency band of 1-10 Hz as representative AF since it is a better overall representation of amplification by the soft sediments than the higher values of 1-5 Hz, as shown in Wassing et al. (2012).

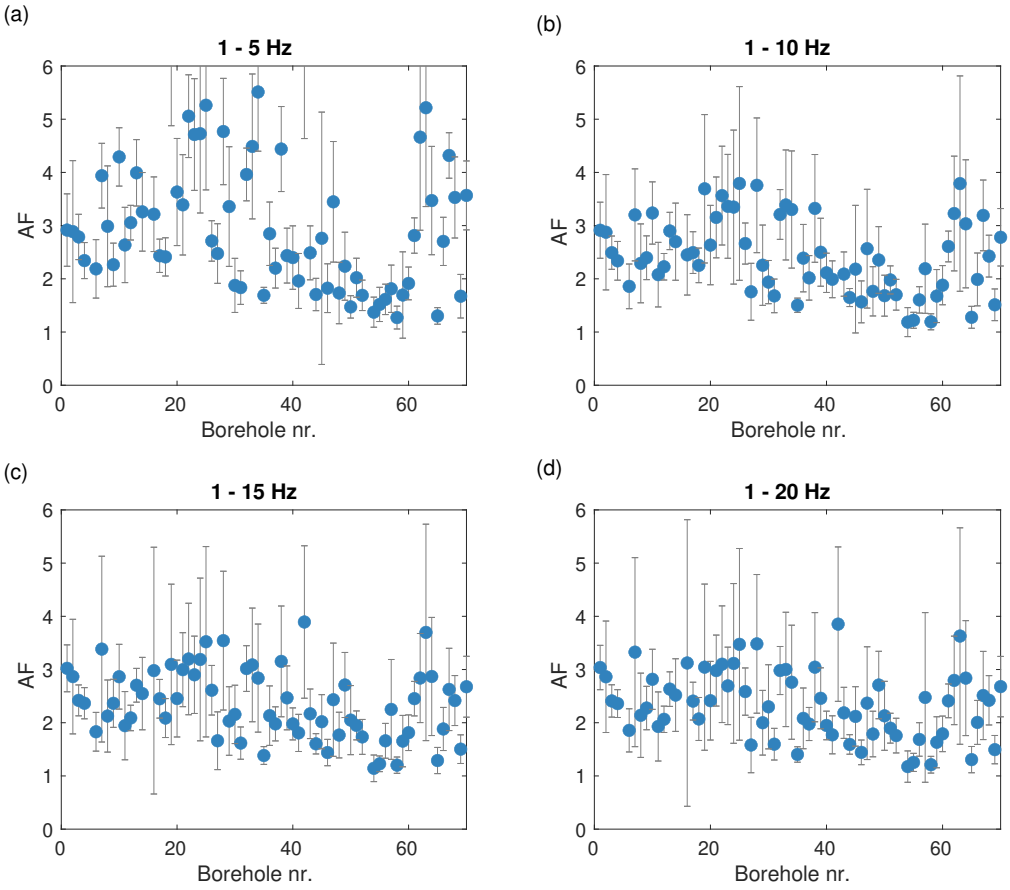

Figure 4. Amplification factors (AFs) for a) frequency band 1-5 Hz, b) 1-10 Hz, c) 1-15 Hz and d) 1-20 Hz and corresponding standard deviations (error bars) associated to the averaged AFs over 19 ~~$M > 2.0$~~ $M \geq 2.0$ local earthquakes.

4.3 Empirical Transfer Functions

We compute the empirical Empirical transfer functions (ETF) represent shear-wave amplification in the frequency domain(in the band 1-10. ETFs are defined as a division of the Fourier amplitude spectra at two different depth levels. With a reference horizon at 200 Hz) from local earthquake motions recorded on the horizontal components of m depth and the level of interest at the Earth's surface, the transfer function has both a causal and acausal part. The causal part maps upward-propagating waves, from the reference level to the borehole seismometers to quantify the maximum shear-wave amplification. Here, we apply the same procedure as described in van Ginkel (2021, vertical component, under review) by taking FAS ratios of earthquake records (0-20surface. The acausal part maps downward-propagating waves back to the free surface (Nakata et al., 2013). When describing amplification, we are only interested in the causal part. We select this causal part of the estimated transfer function and compute its Fourier amplitude spectrum to obtain a measure of frequency-dependent amplification. We use 20 s after earthquake-origin-time) at different depth levels in a borehole for local events with M>2. In this study we compute the ETF between the long time windows for particle velocity recordings on the radial component of the seismometers at surface and at G-network seismometers. Subsequently, we average over 19 local earthquakes with magnitudes ≥2.0. This can be seen as an implementation of seismic interferometry by deconvolution (Wapenaar et al., 2010). Lastly, the deconvolution results are stacked to enhance stationary contributions.

From the ETF between the 200 m depth and surface seismometer (ETF_{200}). From the ETF_{200}, peak amplitudes are identifiedwhich reflect maximum amplification at the corresponding peak frequency. The ETF_{200} derived from the G-network is used for an identification of maximum amplification over the top 200 m that can develop during low magnitude earthquakes. . Some example ETF curves are plotted in Figure 5. Additionally, ETF curves for the top 50 m are calculated (ETF_{50}). The ETF curves for the different intervals show very similar peak characteristics and peak amplitudes, demonstrating that most amplification develops are developed in the top 50 m of the sediment coverwhich is supported by the findings of van Ginkel et al. (2019). Furthermore, the borehole sites with highest ETF peak amplitudes can be linked to the local geology, as presented in van Ginkel et al. (2019, Here, highest peak amplitudes are measured at sites with unconsolidated Holocene alternations of clay and peat, overlying consolidated Pleistocene sediments.

4.4 H/V spectral ratios from the ambient seismic field

The Groningen surface seismometers are continuously recording the ambient seismic field (ASF) and this data is used to estimate horizontal-to-vertical spectral ratios (HVSR). In this study we focus on the second peak (≥ 1 Hz) in the HVSR curve which represents shear-wave resonances at the shallowest interface of soft sediments on top of more consolidated sediments. Resonances of the complete sediment layer display a peak at lower frequencies (van Ginkel et al., 2020). Above 1 Hz the noise field is dominated by anthropogenic sources. Nakamura (1989, 2019) described that the HVSR from ambient noise records is related to the fundamental resonance frequency of the sediment deposits overlying a stiffer bedrock. The details of the method to obtain stable HVSR curves from the ASF in the Groningen borehole network can be found in van Ginkel et al. (2020). In summary, from power spectral densities for each component, the H/V division is performed for each day. Subsequently, a probability density function is computed over one month of H/V ratios and the mean is extracted. This yields a stable HVSR

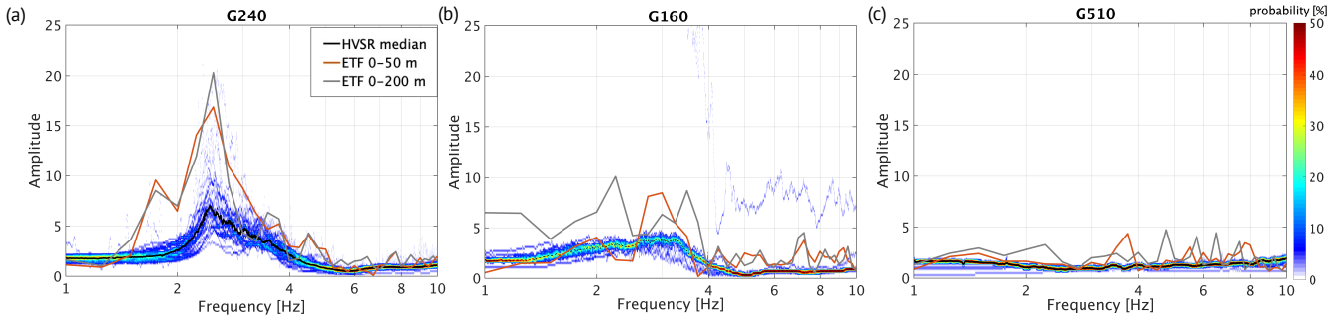

Figure 5. Probability density function of one month of daily HVSRs and the mean HVSR (solid black line) and ETF for the borehole seismometer interval of 0-50 m (gray dashed line) and 0-200 m (gray solid line). The selected borehole sites exhibit differences in curve characteristics with a) G24, illustrating clearly peaked curves (>4). b) G16, illustrating medium (2-4) peak amplitudes. c) G51, no pronounced peak.

curve that is not much affected by transients like nearby footsteps or traffic. ~~van Ginkel et al. (2019) presents the details of this methods for frequencies between 1-10 Hz for the Groningen borehole network.~~

Based on the HVSR curve-and peak characteristics, different criteria are defined conformable to the SESAME consensus (Bard, 2002): 1) Clear peaked curves (HVSR amplitude > 4) related to a sharp velocity contrast in the shallow subsurface. 2) HVSR peak amplitude between 2-4, associated ~~to~~ with a weak velocity contrast. 3) No distinguishable peak and a flat curve indicate the absence of a velocity contrast in the shallow subsurface. Example HVSRs for these three criteria are plotted in Figure 5. Its associated peak amplitudes are derived from the mean HVSR curve and presented in van Ginkel et al. (2019). The correlation between peaks on the HVSR curves and the presence of a velocity contrast at some depth is stressed in studies from Bonnefoy-Claudet et al. (2008), Konno and Ohmachi (1998) and Lermo and Chavez-Garcia (1993) and this contrast is very likely to amplify the ground-motion.

4.5 Amplification parameters

Across the Netherlands, the ASF is continuously recorded on all seismometers, while many locations lack recordings of local earthquakes. Therefore we further investigate whether the HVSR can be used as a proxy for amplification as measured by the earthquake-derived ETF and AF. ~~We do this study with the G-network, where all 3 can be measured (HVSR, ETF and AF).~~ Figure 6 displays the correlation between the peak amplitudes of the HVSR and ETF_{200} as well as HVSR and AF. Secondly, we evaluate the subsurface seismic parameters enhancing amplification (Figure 7).

Based on these data points, relationships are defined in order to be able to estimate amplification factors using HVSR peak amplitudes (A_0), amplification factors:

$$AF = 1.49 + 0.87\log(1.12A_0) \quad (1)$$

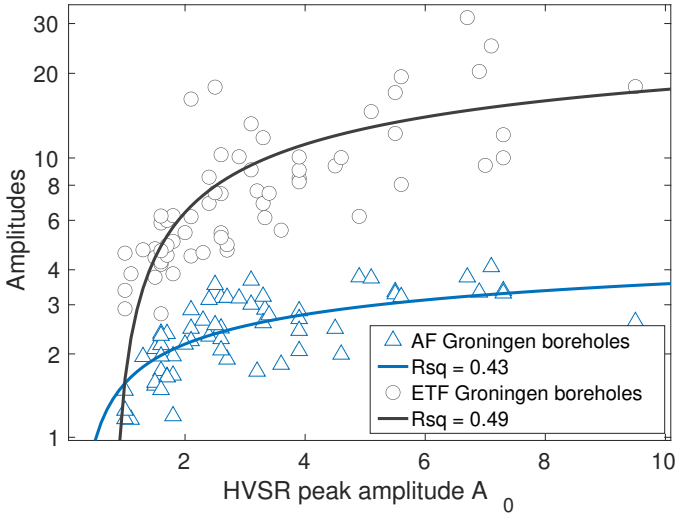

Figure 6. Relation between the HVSR peak amplitudes (A_0) and the ETF peak amplitudes (gray) and the HVSR peak amplitudes and the AF (blue). The solid line represent the fitting function (Equation 1 and 2 between the HVSR peak amplitudes and the measured amplification from AF and ETF, respectively. R_{sq} (R-squared) represents the coefficient of determination of the fitting. Note the log-scale of the y-axis.

and maximum amplification as measured by the ETF:

$$ETF = 1.08 + 6.89\log(1.09A_0). \quad (2)$$

~~Whereas the ETF peak amplitudes represent maximum amplification (at peak frequencies which vary from site to site), the empirical~~ The relationship between the ~~HVSR A_0 and AF is of most importance for the construction of the site-response map. Therefore, the relationship between the AF~~ AF derived from the Groningen borehole locations and local site conditions is investigated in the following.

Many ground-motion prediction equations ~~including~~ which include site-response consider the shear-wave velocity for the top 30 m (Vs_{30}) as the main parameter affecting amplification (Akkar et al., 2014; Bindi et al., 2014; Kruiver et al., 2017b; Wills et al., 2000), as well as Eurocode 8 (CEN et al., 2004). However, ~~recent~~ studies (Castellaro et al., 2008; Kokusho and Sato, 2008; Lee and Trifunac, 2010) have drawn attention to the fact that using only Vs_{30} as proxy for site-response is inadequate, because it does not uniquely correlate with amplification~~, which~~. They show that amplification is defined by several parameters~~like the~~, including the the depth and degree of the seismic impedance contrast. ~~Hence,~~ Furthermore Joyner and Boore (1981) introduce the shear-wave velocity ratio between the top and base layer ~~is introduced~~ as a proxy for site amplification by ~~Joyner and Boore (1981) and~~ is and this is further explored by Boore (2003).

In order to assess the impact of different parameters, ~~first~~firstly, the AF ~~is fitted, using $A_0 = x_1 + x_2 e^{x_3 Vs}$~~ at each borehole location is fitted against several subsurface parameters. Using $AF = a + b * e^{c*Vs}$ as a functional form, where a, b and c are unknown coefficients to be fitted. This fitting is applied with averaged shear-wave velocities over various depth intervals.

Vs_{10}, Vs_{20} and Vs_{30}-values are derived from SCPTs, acquired directly adjacent to 53 borehole sites in Groningen (Figure 2). Hofman et al. (2017) derived interval velocities determined from the G-network, using seismic interferometry applied to local induced events. The velocities from this reference are used to determine Vs_{50}. Secondly, from the SCPT data we derive the depth and size of the velocity contrast~~(VC) by dividing the shear-wave velocity values~~. The contrast is computed by the division of the two different velocity values bounding each 1 m interval. This division is done for each 1 m interval ~~by the maximum value over the full~~ over the 30 m ~~is taken as the VC-value~~of SCPT records. The largest division value is defined as the (main) velocity contrast (VC) and corresponding depth is the depth of the contrast (zVC). Thereafter the VC-values and their depth are fitted with the AF using ~~$A_0 = x_1 + x_2 log(x_3 VC)$~~ $AF = a + b * log(c * VC)$ as a functional form. This procedure is also performed for the relation between the subsurface parameters (Vs, VC) and the HVSR~~and the~~. The results are given in Appendix A.

Figure 7 presents the fit between the AF and the six relevant subsurface parameters. ~~Here, best~~ Best fit (R_{sq}=0.47, Figure 7a,b) is observed between the AF and Vs_{10} and Vs_{20}~~, supporting the findings of Gallipoli and Mucciarelli (2009) by using~~. In line with findings of findings of Gallipoli and Mucciarelli (2009) who use the Vs_{10} as the main amplification parameter instead of the more common Vs_{30}. ~~On the other hand, the correlation between the AF and the VC is less, meaning this parameter is inferior to the AF~~In Groningen, the low-velocity and unconsolidated Holocene sediments have a thickness of 1 to 25 m and below these depths the velocities increase in the more compacted Pleistocene sediments. The reduced fitting quality of the Vs_{30} and Vs_{50} arises since the amplification develops mainly in the Holocene sediments (van Ginkel et al., 2019). Although the fit is relatively poor, a relationship is observable between a large VC and an elevated AF (Figure 7e). By contrast, Figure A1 ~~present~~ presents a good correlation between VC and HVSR. A large VC-value ~~is leading~~ leads to resonance in the near-surface, which is expressed in high amplitude peaks of the HVSR. ~~In the next sections, the VC is still considered as an amplification-determining parameter, however, it obtains a smaller weight than the averaged velocity.~~

5 HVSR estimations throughout the Netherlands

Based on the good relationship between Groningen HVSR peak amplitudes (A_0), ~~the ETF~~ ETF peak amplitudes and AF (Figure 6), we conclude that the HVSR can be further used as proxy for amplification. Therefore, for all surface seismometers in the Netherlands seismic network, the HVSR curves are estimated following the method described in Section 4.4. Figure 8 displays a selection of representative examples of HVSR curves~~, plotted as probability density functions and in solid black the mean HVSR~~. It also includes the sediment classification profile presented in Section 6 and Figure 9. In addition, for boreholes T010, T060 and TERZ, the ETF ~~(red line)~~ curve is added, calculated from local earthquakes similar to the approach described in Section 4.3. These 16 HVSR curves illustrate the diversity in curve characteristics throughout the Netherlands. ~~In general, we~~ Here, we can distinguish the three types of curves as described in Section 4.4. The flat curves with no distinguishable peak (FR040, DRA, T060, T010, WTSB, HRKB, ROLD and BING) are recorded at seismometers on top of outcropping Pleistocene sands (Holocene/Pleistocene eolian and fluvial deposits in Figure 1). Also ALK2 exhibits no peak amplitude since this seismometer is positioned on dune sands (Holocene coastal deposits in Figure 1)~~, with~~. These locations are characterised

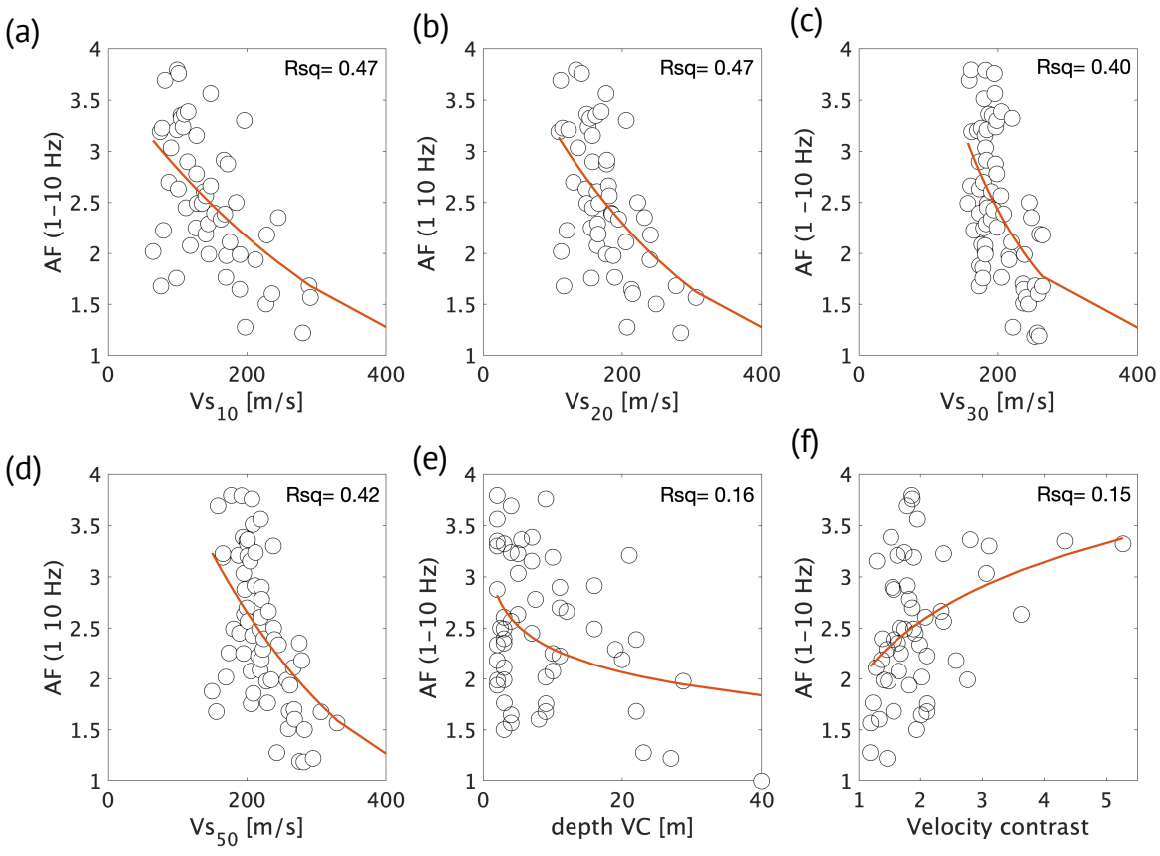

Figure 7. Each panel depicts ~~data points in~~ the ~~G-network, the~~ fitted function and ~~corresponding~~ the coefficient of determination (R_{sq}) ~~between~~ of the AF (1-10 Hz) per G-network borehole location and ~~resp~~the corresponding subsurface parameter. In a) the Vs_{10}, b) Vs_{20}, c) Vs_{30}~~and~~ , d)Vs_{50}, e) depth of the velocity contrast, and e) size of the velocity contrast.

by absence of a strong velocity contrast in the shallow subsurface. Selected examples of HVSR curves exhibiting clear peak amplitudes (NH01,J01, ZH030, FR010, EETW) are located at sites with a distinct velocity contrast between ~~soft~~ unconsolidated Holocene marine sediments overlying Pleistocene ~~sands~~sediments.

~~The~~ In the southernmost part of the Netherlands~~(Zuid Limburg) has a different lithostratigraphic setting compared to the remainder of the country. Here~~, Cretaceous bedrock is either outcropping or situated ~~much~~ less than 100 m deep~~, resulting in soft rock overlying hard rock~~. MAME and TERZ are examples of locations with ~~this setting, hence~~ soft sediments overlying hard rock and the HVSR curves exhibit a clear peak amplitude. ~~For the TERZ borehole the ETF is displaying similar curve characteristics as the HVSR estimations.~~

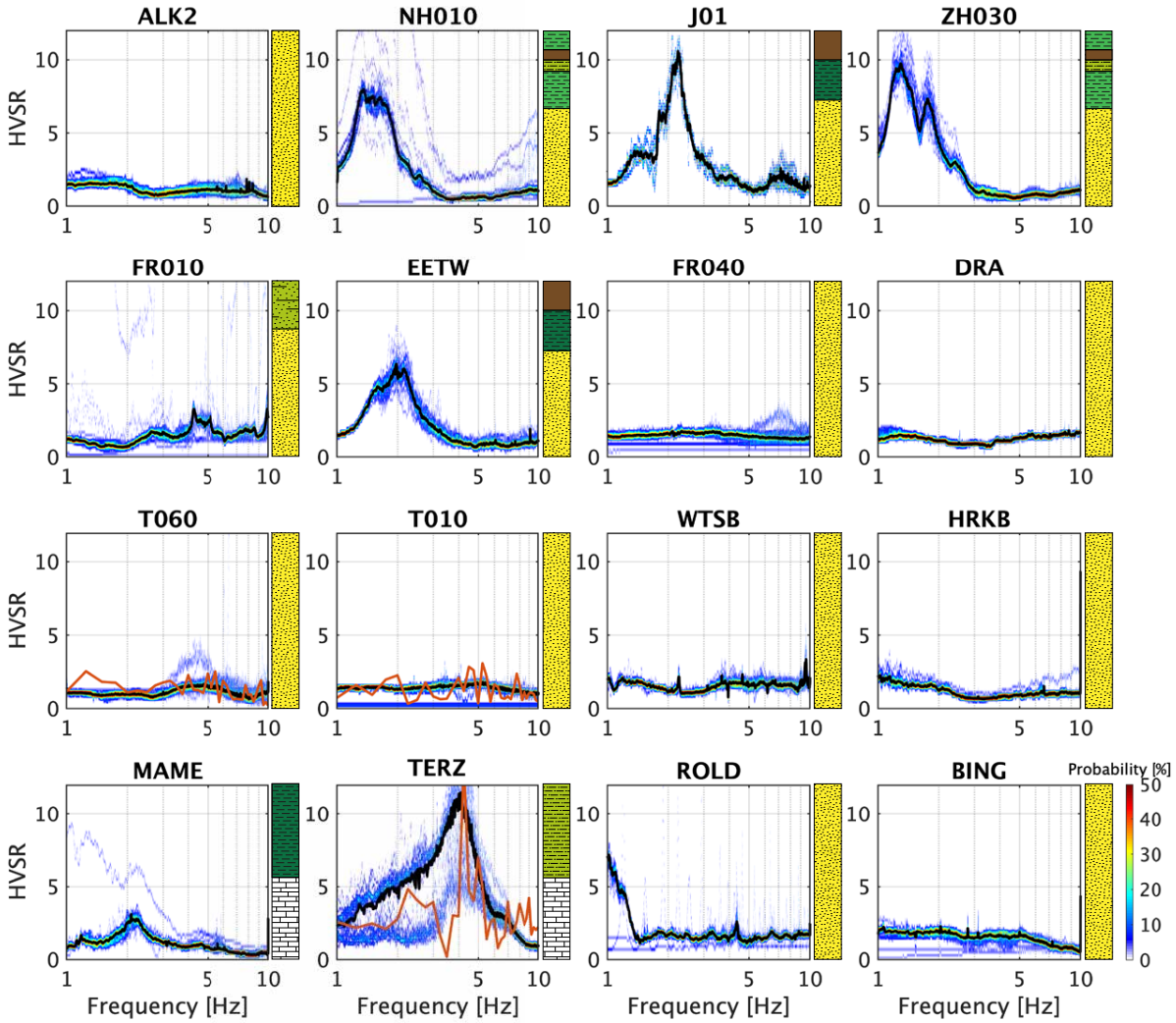

Figure 8. Each panel depicts a probability density function from ambient noise HVSR curves and sediment classification profile (Section 6) for ~~representative~~ 16 stations of the NL-network. The black line represents the mean HVSR ~~. The x-axis is plotted~~ and the red line in ~~log-scale~~the panel of T06, T010 and TERZ represents the ETF calculated from 10 local earthquakes. The color bar in the lower right ~~shows~~ displays the HVSR probability range that is valid for all panels.~~The red line in T06, T010 and TERZ represent the ETF calculated from 10 local earthquakes.~~

6 Zonation map for the Netherlands

~~In this~~ The effect of local site-response on earthquake ground motion is included in the Eurocode 8 seismic design of buildings (CEN et al., 2004, EC8). In order to estimate the risk of enhanced site-response, EC8 presents five soil types based on shear-wave velocities and stratigraphic profiles. Soil-type E is essentially characterised by a sharp contrast of a soft layer overlying a stiffer one. However, in our opinion, this single classification for soft sediments is rather limited, especially concerning the wide variety of lithostratigraphic conditions throughout the Netherlands. Therefore, we present an alternative, or extended, classification for ground characteristics designed to specify the large heterogeneity in site conditions than exists within Eurocode 8 ground-type E.

In this section, in a few steps, the site-response zonation map for the Netherlands is derived. For this, the country is subdivided in grid cells. As a result, about 95% of the grid cells is populated with a site-response class with corresponding AF.

6.1 Classification scheme

The borehole ETFs confirm that most of the amplification ~~develops~~ is developed in the top 50 m (Figure 5) of the sedimentary cover, ~~which is also discussed in van Ginkel et al. (2019). The top 10 m (Figure 7)is most relevant to explain amplification. According to the lithologic class distribution included in GeoTOP and NL3D, most of the amplification appears in the top of the heterogeneous and uncompacted sedimentary cover~~corresponding to the findings in van Ginkel et al. (2019). Beyond 50 m depth, the Quarternary deposits mainly ~~consists~~ consist of more compacted marine and fluvial sediments. Therefore the sediment classification presented in this section uses the top 50 m with a special focus on the top 10 m. Also the presence of a velocity contrast is used in the classification, as it was shown to have a (albeit weaker) link with amplification (Figures 7 and A1).

~~In order to account for the influence of local sediment conditions on seismic ground-motion, the European seismic design of buildings (Eurocode 8; CEN et al., 2004) defines five main soil types, based on lithological description of the sediment column and Vs_{30} (Table 1).~~ Following Convertito et al. (2010) and from the studies by Kruiver et al. (2017a); van Ginkel et al. (2019), the Eurocode 8 classification requires modification, caused by the heterogeneous shallow sediment composition and bedrock depth of the Dutch subsurface. Table 1 lists the criteria for the classification division defined for the Netherlands (NL classification). The NL classification is divided into five classes based on the top ~~20~~50 m lithostratigraphic composition, the velocity contrast (VC) and average shear-wave velocity for the top 10 m.

For setting up the classification we initially use A_0, the peak amplitude from HVSR. ~~The main reason of is that we~~ We only have measured AF in Groningen, whereas we have measured A_0 for many sites ~~over~~ throughout the Netherlands (all stations depicted on Figure 2). Moreover, we found a clear relationship between A_0 and AF (Equation 1).

The relationships between Vs_{10}, VC and A_0 are estimated from lithological conditions ~~as observed~~ in Groningen, where the sites are assigned to Classes II, III and IV. For Classes I and V we have insufficient empirical constraint on A_0 and AF. Only sites with bedrock at depths shallower than 100 m fall into Class V~~. For Class V,~~, for which the resonance over the complete unconsolidated cover can reach frequencies larger than 1 Hz. Therewith, these sites become distinct from Classes II, III and IV, where such resonances occur at frequencies <1 Hz. At these ~~smaller~~ lower frequencies, there is no match with resonance periods of most building types in the Netherlands.

The short lithological description in Table 1 is not sufficient to classify each site. To further aid the classification, representative sediment profiles are obtained (Figure 9) based on the lithologic class sequences of the GeoTOP and NL3D. By grouping the main sediment profiles into the classes, we link the lithostratigraphic conditions to the expected amplification behaviour of the shallow subsurface. The classification is tested and optimized using all the sites with an estimated HVSR curve.

Next step is to attribute a class to each ~~lithostratigraphy~~ lithostratigraphic profile per grid cell in the GeoTOP and NL3D models.

Table 1. Comparison between the Eurocode 8 ground type classification and the sediment classification (NL classification) we present in this paper. The Vs_{10} and velocity contrast (VC) values assigned to each class are based on the amplification relationships presented in ~~section~~ Section 4 and Appendix A. For class V there is no empirical data available relating Vs_{10} and VC with A_0 (HVSR peak amplitude), hence not determined (n.d).

Eurocode 8			**NL classification**				
Ground type	**Description Stratigraphy**	**Vs30 [m/s]**	**Sediment class**	**Description top 200m**	Vs_{10} **[m/s]**	**VC**	A_0
A	Hard rock & rock	>800	**I**	Hard rock	>800	-	-
B	Soft rock & very dense soil	360-800	**II**	Stiff sediment	>200	none or <1.5	<2
C	Stiff soil	180-360	**III**	Soft sediment on stiff sediment	100-200	1.5-2.0	2-4
D	Soft soil	<180	**IV**	Very soft sediment on stiff sediment	<100	>2.0	>4
E	Special soil	<100	**V**	~~Soft sediment~~ shallow bed rock ~~on hard rock~~ (<100 m)	no data	no data	n.d.

6.2 Lithology-based classification

Based on the site-response amplification estimated with the HVSR peak amplitudes at 115 sites, we have categorized each sedimentary profile (Figure 9) into a class. Next step is to substitute GeoTOP and NL3D into these five classes. This ~~geological~~ geologically based method allows the determination of site-response on regional and ~~national~~ nation-wide scale. Figure 10 gives a general outline of the procedure used to assign the appropriate sediment class to each of the voxel-stacks in GeoTOP and NL3D. A voxel-stack is the vertical sequence of voxels at a particular (x,y)-location in GeoTOP or NL3D. Details on each of the processing steps are given in Appendix C. Next step is to attribute an amplification factor to each class.

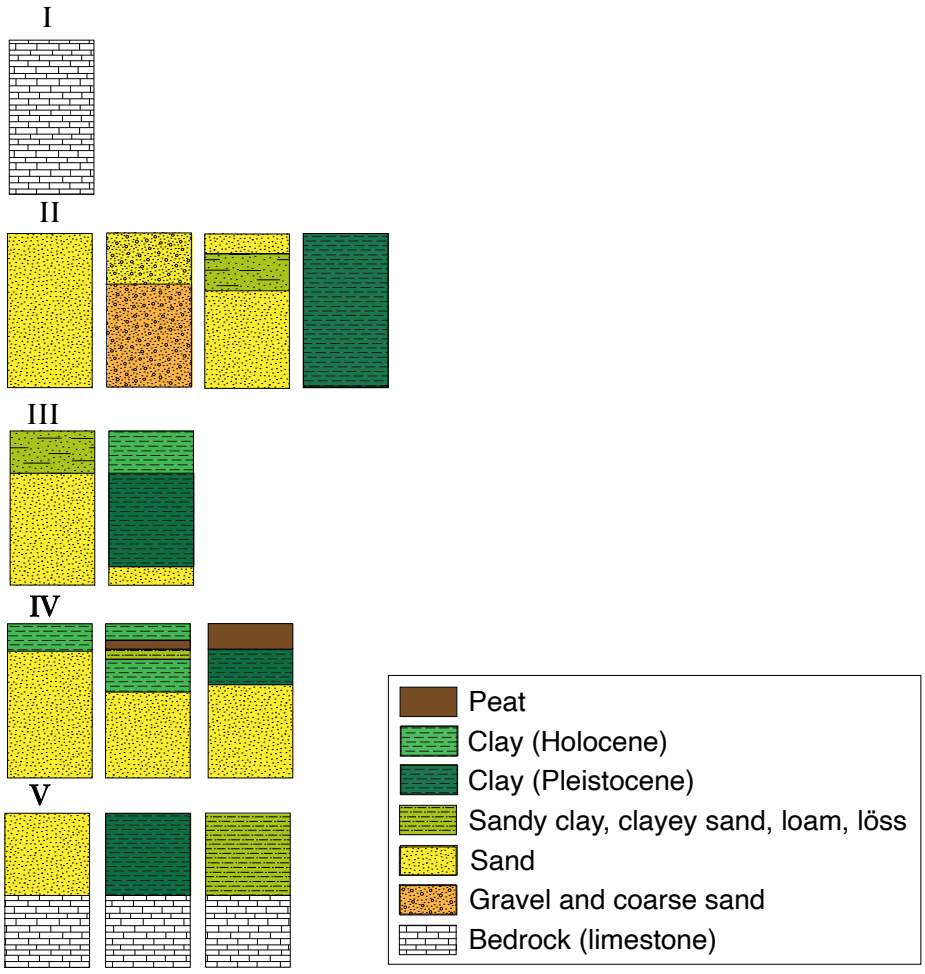

Figure 9. Sediment profiles corresponding to the classification presented in Table 1, where the different columns are typical examples of the top 50 m of the Netherlands. The division in classes is based on the shallow subsurface composition related to the expected level of wave amplification during a seismic event.

6.3 Amplification factors for the Netherlands

For shake-map implementations or seismic hazard analysis, amplification factors (AF) are usually derived from the Vs_{30} (e.g. Borcherdt (1994)). In this study, we estimate AFs by substituting the HVSR peak amplitudes (A_0) for 115 stations throughout the Netherlands into Equation 1. This allows the calculation of ~~nationally~~ nation-wide applicable AF-values (AF_{NL}) assigned to each of the classes presented in Figure 9.

In order to obtain an AF_{NL} for each class, the 115 calculated AFs are plotted against their site sediment class in Figure 11a. For these 115 locations, the sediment classes are manually assigned based on the geological models, SCPT or other geological data available. From the AF distributions, the mean AF-values (AF_{NL}) and corresponding standard deviation (σ_{AF})

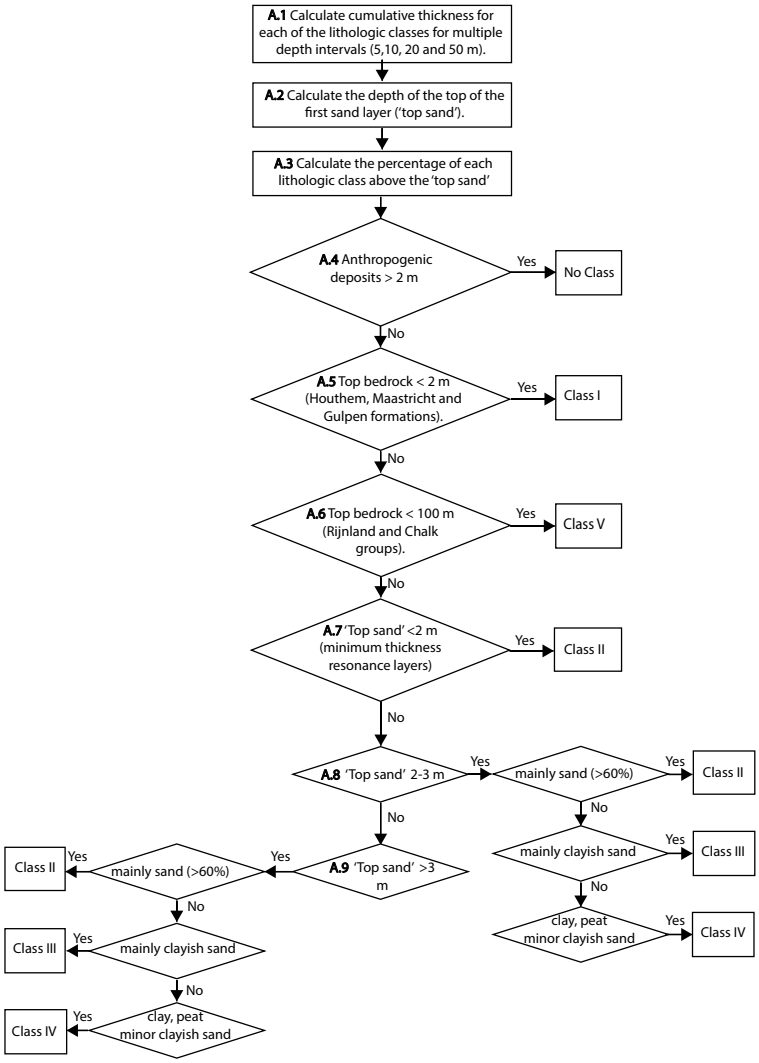

Figure 10. General outline of the vertical voxel-stack analysis used to assign the appropriate sediment class into each grid cell of the GeoTOP and NL3D geological models in the construction of the site-response zonation map.

are calculated for each class (Table 2). In Class II there are a number of sites with exactly the same AF of 1.6. These are sites with no distinguishable peak, where A_0 is set to 1, which yields, after filling out in Equation 1, AF=1.6.

The AF_{NL}-values are valid on a national scale for a frequency range of 1-10 Hz and for reference ~~rock~~ conditions of Vs =500 m/s (Section 4.1). There are no AF values for sites in the farthest south and east of the Netherlands, so these areas fall into Classes I and V. There is too little data to calibrate the corresponding amplification factor.

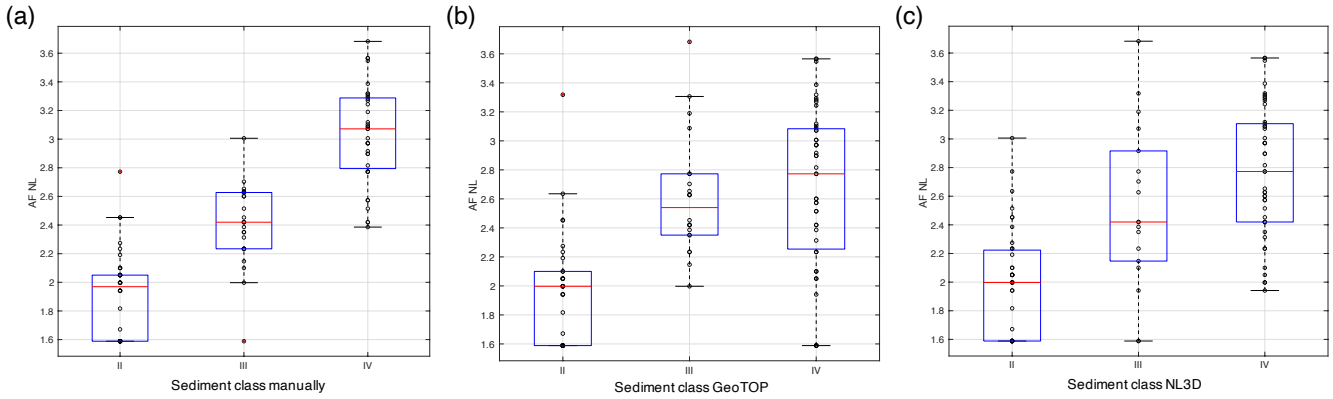

Figure 11. Comparison of calculated AF distribution in terms of manual classification (a), automatic classification by GeoTOP (b) and by NL3D (c). The locations where the empirical AF relationship is not valid are eliminated (class I and V). The red central mark indicates the median; the bottom and top edges of the box indicate resp. the 25th and 75th percentiles. The whiskers extend to the most extreme data points and the outliers (1.5x away from the interquartile range) are plotted individually as red circles.

By applying the workflow that we introduced in Section 6.2, automatic classification for the 115 sites is performed based on resp. GeoTOP and NL3D and plotted against the AF (Figure 11b and c). Due to uncertainties in the models (Appendix C), these distributions deviate from the manual classification (Figure 11a). Note that for the manual classification, e.g., SCPT information could be used at 53 sites, which local information is not included in GeoTOP and NL3D. We therefore distinguish two types of uncertainty:

1. σ_{AF}: this is the variability that ~~comes~~ originates from the classification. Within the classification, a number of different sites is binned into the same class (Figure 9) although in reality there is still a range of amplification behavior. This variability is approximated with the outcome of the manual classification (Figure 11a), which could be done in great detail.

2. σ_{mod}: the geological models are geostatistical models where not all grid cells contain individual lithological data. Hence, there is an uncertainty of the actual lithological succession at each grid cell. The total uncertainty σ_{tot} (derived from Figure 11b,c) can be written as $\sqrt{\sigma_{AF}^2 + \sigma_{mod}^2}$. By additionally averaging over the classes (labeled with subscript $_i$) we find the model uncertainty σ_{mod}:

$$\sigma_{mod} = \frac{1}{n}\sum_{i=1}^{n}\sqrt{{\sigma_{tot,i}}^2 - {\sigma_{AF,i}}^2}. \tag{3}$$

Table 2 lists the mean AF values, the uncertainty in AF (σ_{AF}) and the uncertainty (σ) for the GeoTOP and NL3D models.

Table 2. Amplification factors and standard deviations (σ) for the NL classification. σ_{AF} is the uncertainty when a local (HVSR) recording is available. σ GeoTOP and σ NL3D represents the additional uncertainty associated with the GeoTOP and NL3D models.

Class	AF_{NL}	σ_{AF}	σ GeoTOP	σ NL3D
II	1.94	0.30	-	-
III	2.4	0.28	0.32	0.34
IV	3.03	0.34	-	-

6.4 Site-response zonation map

The workflow presented in Figure 10 results in a class category assigned to each grid cell of the GeoTOP and NL3D models. As a result, we present the national site-response zonation map (Figure 12), ~~were~~ where each class characterises a certain level of expected site-response amplification. ~~Each~~ Additionally, each class has an AF_{NL} assigned (Table 1). Figure 13 presents four zoom-in panels of the map, each depicting a region of particular interest.

Some areas show a large scatter in classes, which is derived from a large heterogeneity in the near surface as represented in the lithostratigraphic models. Typically, at these places there is large model uncertainty~~. For~~ , for example in north-east Noord-Holland (Figure 13a). Here, the Holocene lithological successions are very ~~heteogeneous~~ heterogeneous in terms of clay, peat and clayish sand. This region also exhibits discrepancies between the model's lithological successions and HVSR curve characteristics, for instance with seismometers J01 (Figure 8) and J02. The geological model at these locations presents large portions of clayish sand, resulting in class category III, while the HVSR curves exhibit distinctive, high amplitude peaks, demonstrating local conditions related to class IV.

For larger sedimentary bodies, like the dune area, there is less model uncertainty. Dune sand is identified as class II, and here, the HVSR of the seismometers (e.g. ALK2, Figure 8) deficit any peak due to the absence of ~~an~~ a velocity contrast in the near-surface.

Figure 13b covers the "Randstad" region, most densely ~~urbanize~~ urbanized part of the Netherlands, where the class is mainly determined as IV. Figure 13c shows the southeastern part. Most of the northern part of this region is Class II due to Pleistocene sands reaching the surface. Most of the southern part of this region falls into Class V since the bedrock occurs at depth less than 100 m. A few places with bed rock outcrops fall into Class I.

Since Groningen has been studied in much detail, we also present the site-response zonation for this region (Figure 13d), and discuss this in Section 7.

7 Discussion

The seismic site-response zonation map presented in Figure 12 distinguishes five classes, each of which defining the potential of occurrence of the related site-response amplification. Here, the lithological conditions are collated into zonations (classes) using the classification as shown in Figure 9. In the development of the lithostratigraphically based classification, we used

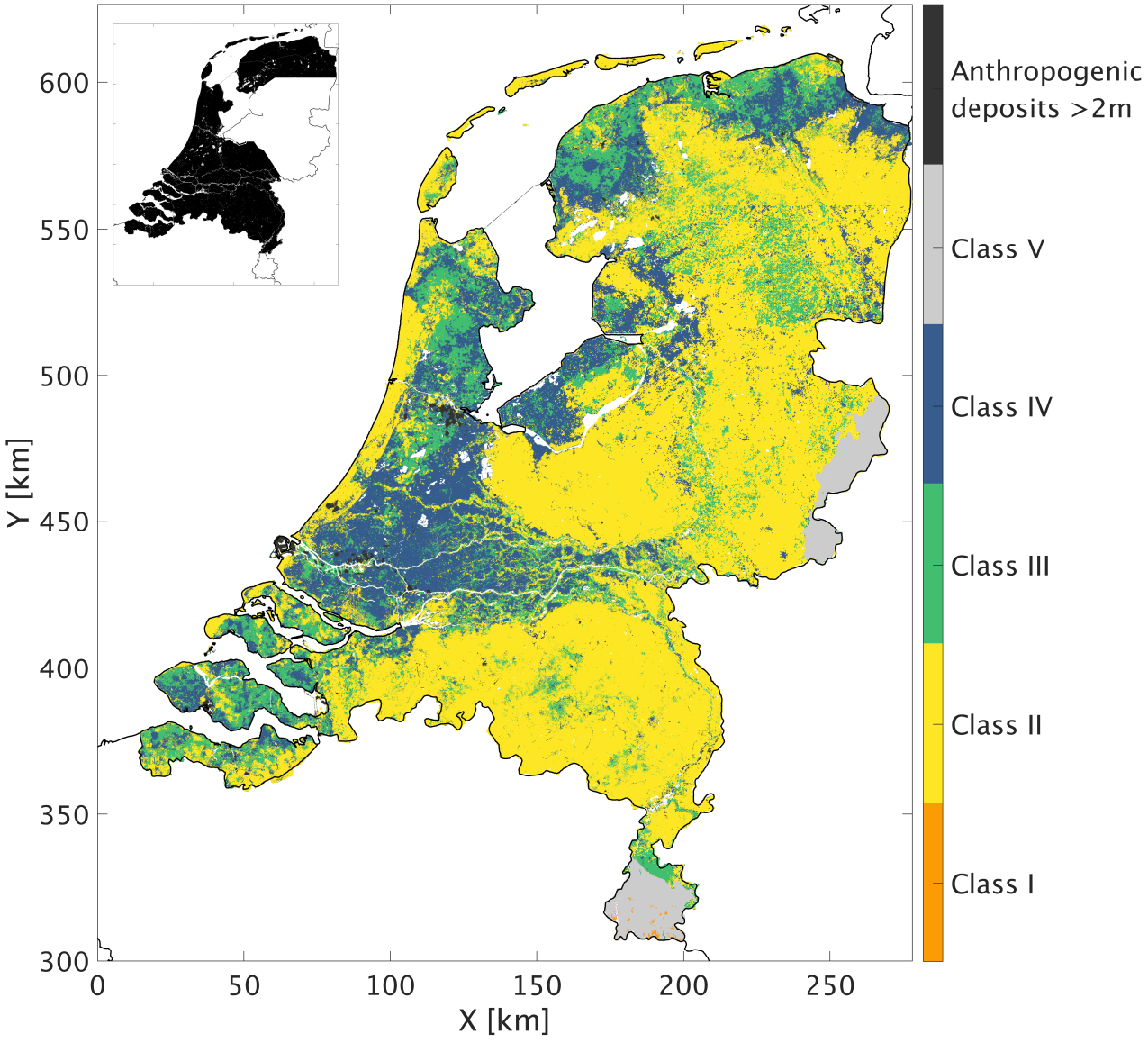

Figure 12. Seismic site-response zonation map for the Netherlands designed for low-magnitude induced earthquakes. The GeoTOP model coverage is highlighted in black in the small inset. For the remaining part of the Netherlands, the NL3D model is used as foundation for the classification. The white spots are water bodies. The amplification factors and related uncertainties are presented in Table 2.

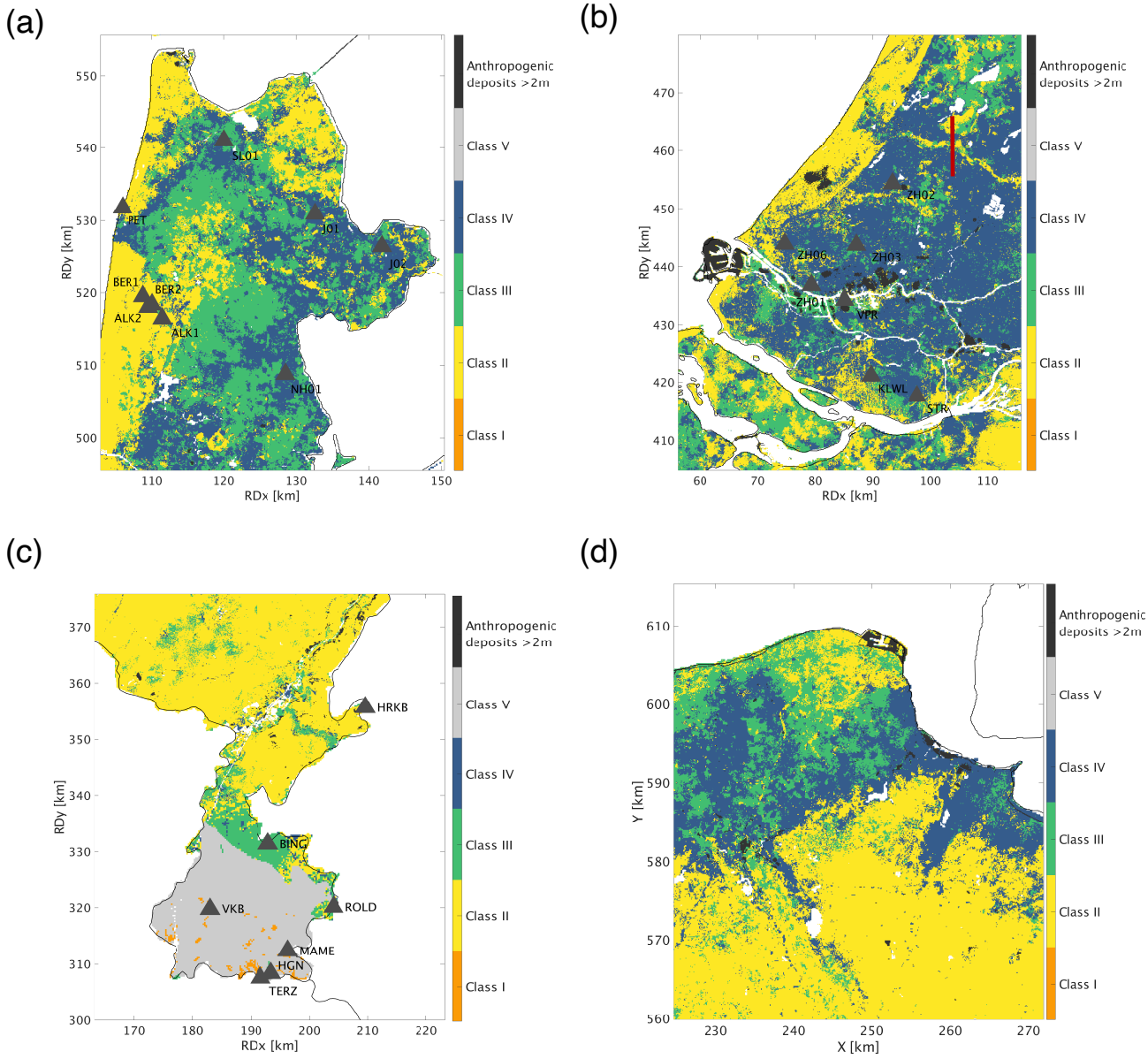

Figure 13. Panels highlighting different regions in the site-response zonation map, including the seismometer locations. a) Noord Holland: with a heterogeneous pattern between class III and IV, b) The densely urbanized area of Zuid Holland, the red line indicates the S-N cross-section through the GeoTOP voxel model (Figure C1). c) Limburg ~~: which~~ is in the north a quite homogeneous zone of class II, while the south is dominating by class I and V due to shallow and outcropping bedrock. d) North-east Groningen is added as comparison to other studies performed in that region. No seismometer locations are plotted here because of the high density covering the map.

i) HVSR peak amplitudes, ii) the presence of a velocity contrast at depth, iii) shear wave velocities. Amplification factors are assigned to each class. In the following paragraphs we discuss the validity and uncertainties of the classification, the AF distributions, as well as the usage and limitations of the presented map.

Since the ambient noise sources in the frequency band of interest (1-1 Hz) partly have an anthropogenic origin, one should be careful about contamination by local strong noise because it may seriously affect the amplitude of the HVSR as shown in Guillier et al. (2007); Molnar et al. (2018). We resolved this problem by using large portions (30 days) of noise data to create stable HVSR curves (van Ginkel et al., 2020). It is important to mention the qualitative character of the microtremor HVSR peak amplitudes which in itself do not directly relate to the amplification of a signal at the surface during an earthquake. However, the microtremor HVSR curve characteristics show major similarities with the measured amplification from earthquake ETFs (Figure 5), but not in terms of absolute values. Therefore an additional fitting-relationship (Equation 1) has been defined, suitable to use the microtremor HVSR peak amplitudes as proxy for amplification. HVSR measurements have proven to be very informative for site-response estimation and remain a valuable input for seismic site-response zonation (Molnar et al., 2018; Bonnefoy-Claudet et al., 2009).

Considering the difficulty in observing sufficient numbers of earthquake ground-motions in areas that are not seismically active, or where no large seismic networks are available, we resorted to deriving and calibrating a lithology-based classification scheme. We took advantage of the detailed models of Cenozoic lithostratigraphy which are available in the Netherlands. As a consequence, the site-response map (Figure 12) exhibits ~~an~~ a regional pattern which is rather similar to the geological map (Figure 1). We showed that the use of these models yields additional uncertainty in the determination of the AF (Table 2). This uncertainty of the actual lithostratigraphic profile at a site can be circumvented by a local recording. This may be an HVSR to obtain more certainty on the site effect (Table 1), a cone-penetration test (CPT) to obtain constraints on the lithology, or, better still, a seismic cone penetration test (SCPT) to get a local ~~S-wave~~ shear-wave velocity profile.

Rodriguez-Marek et al. (2017) defined a site-response model including magnitude and distance dependent linear amplification factors (AF_{Gr}) for several period intervals (0.01-1.0 s) for the Groningen region as input for ground-motion prediction equations by Bommer et al. (2017). This site-response model starts from a reference horizon at the interface between the unconsolidated sediments and the stiffer Chalk formation below at around 800-1000 m depth. However, this contrast is both variable in depth and value throughout the Netherlands and therefore not easily applicable as a reference horizon for the purpose of our study. ~~Rodriguez-Marek et al. (2017) presented model-based AFs (AF_{Gr}) for several periods in the range of 0.01-1.0 s.~~ The class-dependent AF_{NL} presented in this paper is defined against a reference rock with a velocity at 500 m/s (which in Groningen is situated at 200 m depth). Therefore the AF_{Gr} cannot be directly be quantitatively correlated to the AF_{NL}; this requires a correction which includes the transmission coefficient calculated at the base of the North Sea Group and a damping model. By ignoring the absolute values and comparing both AFs qualitatively, the overall spatial distribution of AF_{NL} in the Groningen region (Figure 13d, in a frequency band 1-10 Hz) corresponds best with AF_{Gr} at a spectral period of 0.01 s (Figure 10; Rodriguez-Marek et al., 2017). This is in line with or findings that AFs do not change much anymore when frequencies above 10 Hz are included (Figure 4).

7.1 Usage of the site-response zonation map

The map presented in Figure 12 enables a prediction of site-response after a local earthquake as recommended in the following. It is very important to note that lithological information from geological voxel models is based on spatial interpolation and aimed at interpretations on regional scale. As a consequence, the presented site-response zonation map is also designed for regional interpretation, ~~but~~ and not on individual grid cell scale. Furthermore, at locations with large subsurface heterogeneity, the interpretation should be handled with care. Additional local investigations like SCPT measurements should be performed at sites of interest in order to assess the site-response in detail.

For the map presented, the uncertainties to keep in mind are: first, the AF distribution along the classes (Figure 11a), and secondly the uncertainty of the geological model used (σ GeoTOP and σ NL3D, Table 2). The AF_{NL} is designed to be added to an input seismic signal ~~with reference seismic bedrock conditions with a shear wave~~ at a reference horizon with a shear-wave velocity of 500 m/s. This AF_{NL} is class-dependent and covering only frequencies of 1-10 Hz. Furthermore, the AF_{NL} including the σ_{AF} does not reflect the maximum amplification that might occur within a smaller frequency band.

The frequency content of large tectonic-related earthquakes differs from induced tremors. The national AF is based on low-magnitude induced earthquakes and incorporates a frequency range of 1-10 Hz. In case of a strong tectonic earthquake, frequencies below 1 Hz start to play a role and resonances with deeper velocity contrasts (>100 m) which are not reflected in the current AF_{NL} might become important. Also, for very strong ~~ground-motion~~ground-motions, which would occur in the epicentral area of large-magnitude tectonic events, non-linearity and distance dependence could become important (Bazzurro* and Cornell, 2004; Kwok et al., 2008). Both effects have not been included in the derivation of the AF_{NL}. Moreover, in the country's southern regions, a topographic effect may influence the site-response. It is important to mention that for now these areas are aggregated in Class V and require additional detailed site investigations for site-response assessment.

8 Conclusions

In this paper we presented a workflow to create a nationwide site-response zonation, using lithological sequences as proxy for seismic site-response. To that end, we first analysed the observed earthquake and ambient seismic field recorded at 69 stations of the Groningen borehole network in order to obtain empirical relationships for amplification. Based on the shallow subsurface resonance frequencies and earthquake amplitude spectra, the earthquake and ambient noise frequency band-pass filtering was applied in the range 1-10 Hz. Derived from the Groningen empirical relationships, we showed that the horizontal-to-vertical spectral ratio (HVSR) approach provides a simple means of determining the amplification potential for most subsurface conditions in the Netherlands. In a second stage, we determined the HVSR curves for additional 46 surface seismometers throughout the Netherlands and calculated the subsequent peak amplitudes. These peak amplitude distributions were related to specific lithological profiles and amplification factors. With the accrued knowledge of amplification potential of different lithological sequences, a classification scheme was designed. This turned out to be a useful tool for translation of the grid cells of the geological models into five classes, and therewith establishing a national site-response zonation map. Most classes have an AF_{NL} assigned, which values can be added to input seismic responses adhering the reference seismic bedrock conditions.

Class I are sites with a hard rock setting. These sites can only be found in the very south and east of the Netherlands. An amplification factor (AF) of 1, meaning no amplification, is assigned to these locations. Class II is associated to sites with stiff sands or Pleistocene clays without strong impedance contrasts in the near surface. One may expect only small amplification at these sites. Class III are sites with relatively soft sediments (clays, sandy clays, löss) overlying stiffer sands, resulting in impedance contrasts in the near surface. Class IV is related mostly to very soft and unconsolidated Holocene clay and peat successions overlying stiffer sands, forming a strong impedance contrasts. At these sites, the largest amplification occurs. Class V are sites at which the bedrock occurs shallower than 100 m, which is not very common in the Netherlands. For these sites there was insufficient data to assign an amplification factor.

Some limitations exist in this study. The method and map proposed is not applicable to regions with strongly deviating lithological sequences, or for earthquakes with very strong low-frequency (f<1 Hz) shaking.

Finally, it is worth noting that the proposed map could be improved by i) adding new site geotechnical data like SCPTs, ii) including updates and extensions of GeoTOP, iii) including amplification factors derived from new KNMI stations and iv) adding new records of earthquake motions to constrain amplification factors for class V.

Appendix A: HVSR amplification parameters

In this appendix, HVSR peak amplitudes (A_0) are fitted with the six parameters that influence ground-motion site-response (Figure A1). Best fit (R_{sq}=0.39) is observed between A_0 and Vs_{10}. Hence, the Vs_{10} is used for further correlation purposes instead of the more common Vs_{30}, supporting the findings of Gallipoli and Mucciarelli (2009) by using the Vs_{10} as main amplification parameter. The depth of the first strong velocity contrast (VC, which is defined within the top 50 m) has a poor relation with A_0 (Figure A1e). The size of the velocity contrast, however, does have a strong relation with A_0 (Figure A1f).

Compared to individual 1D correlations, a 2D correlation (Figure A2) using both the VC and the Vs_{10} results in an improved correlation (R_{sq}=0.53) and allows to define an empirical relationship for HVSR peak amplitudes (A_0) based on these two parameters:

$$A_0 = -1.29\log(0.01Vs_{10}) + 0.99VC + 1.94 \quad \text{(A1)}$$

Furthermore, this equation supports the hypothesis of Joyner and Boore (1981); Boore (2003) that A_0 is depending on also the VC. The motivation for equation A1 is to achieve an amplification equation based on subsurface parameters only. Using equation A1 an estimate is obtained of A_0. Subsequently, Equation 1 can be used to obtain an estimate of the amplification factor.

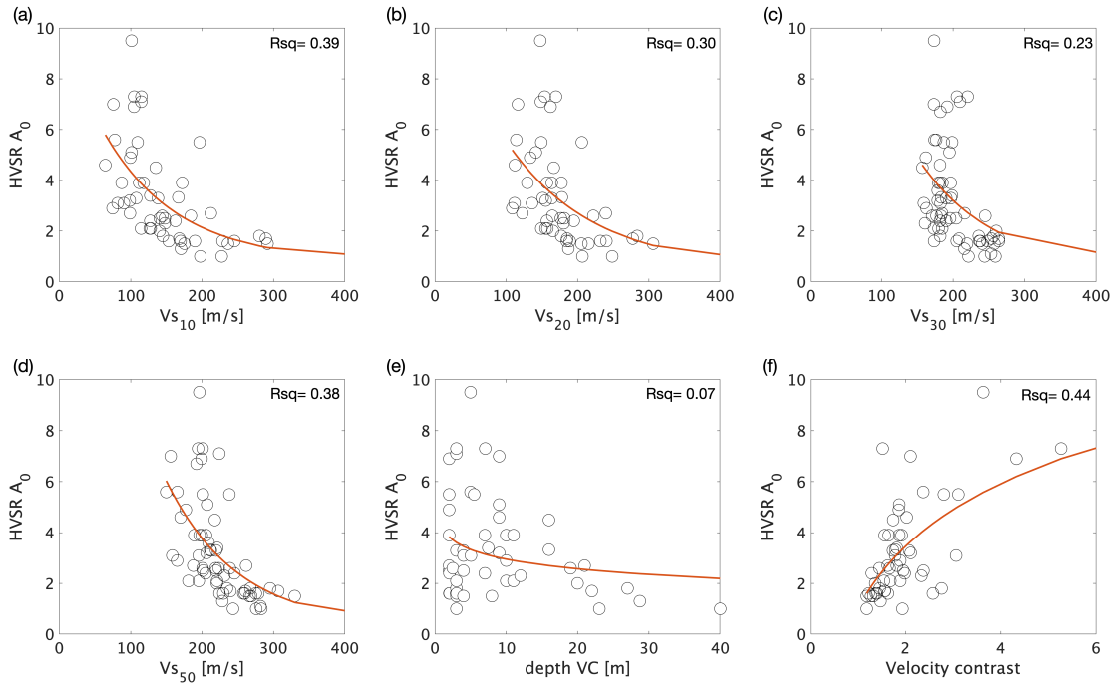

Figure A1. Each panel depicts ~~data points of~~ the ~~G-network,~~ fitted function and ~~corresponding~~ the coefficient of ~~determination~~ determinations (~~R_{sq}~~ Rsq) ~~between~~ of the HVSR peak amplitude A_0 per G-network borehole location and ~~resp~~the corresponding subsurface parameter. In a) the Vs_{10}, b) Vs_{20}, c) Vs_{30} ~~and~~ , d) Vs_{50}, e) depth of the velocity contrast, and e) size of the velocity contrast ~~(VC)~~.

Appendix B: Geological models

B1 GeoTOP

GeoTOP schematizes the shallow subsurface of the Netherlands in voxels measuring 100 by 100 by 0.5 m (x ,y, z) up to a depth of 50 m below ordnance datum (Stafleu et al., 2011, 2021). Each voxel contains estimates of the lithostratigraphic unit the voxel belongs to and the lithologic class (including a sand grain-size class) that is representative for the voxel. GeoTOP is publicly available from the web portal of TNO – Geological Survey of the Netherlands (GDN; https://www.dinoloket.nl/en/subsurface-models). GeoTOP is constructed using some 275,000 borehole descriptions from DINO, the national Dutch subsurface database operated by GDN (https://www.dinoloket.nl/en/subsurface-data), complemented with some 125,000 borehole logs from Utrecht University in the central Rhine-Meuse river area. The modelling procedure involves four steps: First, the borehole descriptions are interpreted into standardized lithostratigraphic units with uniform sediment characteristics. Given the large number of boreholes, automated lithostratigraphic interpretation routines (Python scripts) were developed. These routines combine digital maps, stratigraphic rules (e.g. superposition) and lithologic criteria (e.g. main lithology, admixtures, grainsize and shell

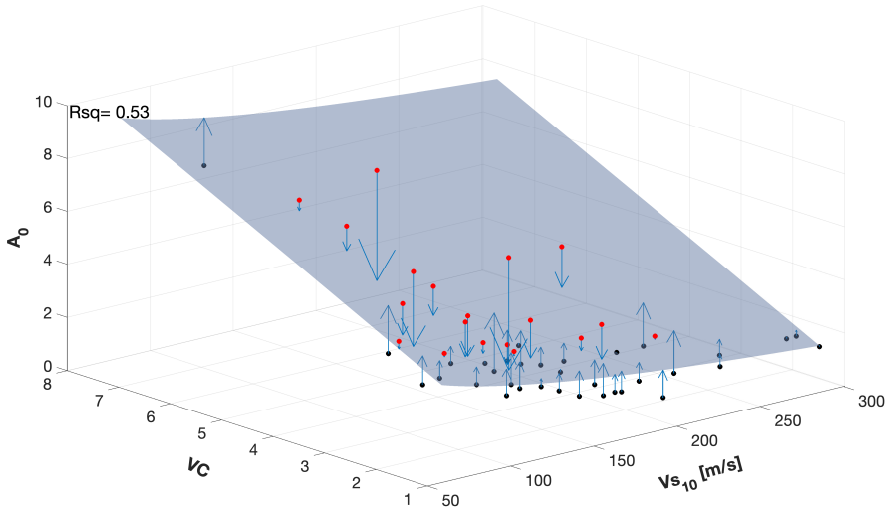

Figure A2. 3D-Plot of the two main parameters that define amplification; the velocity contrast and Vs_{10}. The pale blue surface depicts the fitting function between the parameters and divides the data points where the red points are above the surface and black points below. Blue arrows indicate the difference (error) between the surface and data point.

content, amongst other criteria) to determine the depth of the top and base of the lithostratigraphic units in each of the borehole descriptions. Next, 2D interpolation techniques are used to construct surfaces bounding the bases of the lithostratigraphic units as observed in the boreholes. The interpolation algorithm allows for the calculation of a mean depth estimate of each surface and its standard deviation. Subsequently, all surfaces are stacked according to their stratigraphical position, resulting in a consistent layer-based model with estimates of top and base of each lithostratigraphic unit. Top surfaces are derived from the bases of the overlying units. The surfaces are then used to place each voxel in the model within the correct lithostratigraphic unit. In the third step, the borehole descriptions are revisited and classified in six different lithologic classes ('peat', 'clay', 'clayey sand & sandy clay', 'fine sand', 'medium sand' and 'coarse sand and gravel'). In the last modelling step, a 3D stochastic simulation is performed for each lithostratigraphic unit separately. The simulation results in 100 equiprobable realizations of lithologic and grain-size class for each voxel. Post-processing of the realizations results in probabilities of occurrence as well as a 'most likely' estimate of lithologic and grain-size class. This 'most likely' estimate is used in the construction of the seismic site-response zonation map (Appendix C).

B2 NL3D

To date, the GeoTOP model covers about 70% of the country (including inland waters such as the Wadden Sea). For the missing areas we have used the lower-resolution voxel model NL3D, which is available for the entire country (Van der Meulen et al., 2013). NL3D models lithology and sand grain-size classes within the geological units of the layer-based subsurface

model DGM (Gunnink et al., 2013) in voxels measuring 250 by 250 by 1 m (x ,y, z) up to a depth of 50 m below ordnance datum. NL3D uses a much simpler modelling procedure than GeoTOP: First, the borehole descriptions are interpreted by intersecting each borehole with the top and base raster layers from the DGM model. The resulting stratigraphical interpretations are geometrically consistent with the DGM model, but not necessarily consistent with the borehole descriptions (e.g., a borehole interval describing 'sand' may erroneously fall within a unit that is characterized by clay deposits). Second, the surfaces of the DGM model are used to place each voxel in the model within the correct lithostratigraphic unit. DGM is a layer-based model using a smaller dataset of some 26,500 manually interpreted borehole descriptions from the DINO database. Consequently, it is less refined than GeoTOP. For instance, DGM combines all Holocene formations in a single unit, whereas GeoTOP features some 25 different Holocene formations, members and beds. The third and fourth steps are identical to the ones described for GeoTOP. The resulting NL3D model has a similar 'most likely' estimate of lithologic and grain-size class which is used in the construction of the seismic site-response zonation map (Appendix C).

B3 Model uncertainty

The current version of GeoTOP covers about 28,605 km^2 using some 400,000 boreholes. This implies that only about 7% of the voxels at land surface contain a borehole. Moreover, this number rapidly decreases with depth because many boreholes are quite shallow. Therefore, the lithostratigraphic unit and the lithologic class of almost all voxels are estimated on the basis of nearby borehole descriptions. As a 'rule-of'-thumb', the limited amount of data available deeper than 30 m below land surface strongly reduces the quality of the lithologic class estimates of GeoTOP (Stafleu et al., 2021). For NL3D, this number is 15 m.

B4 Applicability

GeoTOP and NL3D model the subsurface at a regional to subregional scale that is suitable for applications at the levels of province, municipality and district. The models are not suited for applications that require a finer scale at the level of streets or individual buildings.

Appendix C: Workflow site-response map

The steps below describe the procedure used to assign the appropriate sediment (site-response) class to each of the voxel-stacks in GeoTOP and NL3D, as exemplified in Figure C1. A voxel-stack is the vertical sequence of voxels at a particular (x,y)-location in GeoTOP or NL3D. At each voxel there is an estimate of the lithostratigraphic unit and the lithologic class (Appendix B).

- **A.1** Calculate the cumulative thickness for each of the lithologic classes ('peat', 'clay', 'clayey sand ~~and~~ & sandy clay' and 'sand') in the models for multiple depth intervals (5,10, 20 and 50 m). The thicknesses of the lithologic classes 'fine sand', 'medium sand' and 'coarse sand gravel' have been added together in the superclass 'sand'.

- **A.2** Calculate the depth of the top of the first consecutive sequence of sand with a minimum thickness of 1.5 m (GeoTOP) or 2 m (NL3D). This depth is further referred to as 'top sand'. In general, 'thick' sequences of sand represent the stiffer Pleistocene sediments. In other cases, they may represent Holocene sediments of, for example, the fluvial channel belt systems of the Rhine and Meuse, or the coastal dunes. These sands form the contrast with the overlying soft sediments ('peat', 'clay' and 'clayey sand and sandy clay'). Voxel-stacks containing a continuous Pleistocene clay sequence (Elsterian tunnel valleys) are included in the depth of the first sand (top sand), since no amplification is estimated here with the HVSR of site N02.

- **A.3** Calculate the percentage of each lithologic class above the 'top sand'. These percentages play an important role in assigning sediment site-response classes as described in steps **A.8** and **A.9**.

- **A.4** If anthropogenic deposits reach up to depths larger than 2 m, no sediment class is assigned. Anthropogenic activities have modified the near-surface composition at many locations in the urbanized areas of the Netherlands. The lithologic class of these sediments is unknown. Therefore, we are not able to assign a sediment site-response class to those locations.

- **A.5** If bedrock outcrops or occurs at a depth smaller than 2 m, the site is assigned to Class I. The depth criterion is set at a maximum of 2 m since a deeper top bedrock would lead to a top layer with a possible resonance in the 1-10 Hz frequency band and hence a different site-response class. The top of the bedrock is determined from the DGM model (Gunnink et al., 2013) (top surfaces of the Houthem, Maastricht and Gulpen formations).

- **A.6** If bedrock in the eastern and southern part of the country occurs at a depth smaller than 100 m, the sediment site-response class is set to V. These are sites where the layer on top of the bedrock could yield a resonance in the 1-10 Hz band, which resonance has not sufficiently be calibrated to assign an AF_{NL}. Class V thus corresponds to sites with a currently unknown amplification potential. The top of the bedrock is determined from the DGM-deep model (Gunnink et al., 2013) (top surfaces of the Rijnland and Chalk groups).

- **A.7** If 'top sand' is less than 2 m, the site-response class is set at II. Examples of HVSR curves with 'top sand' less than 2 m, do not exhibit any peak amplitude due to the absence of a resonating soft layer on top of a stiffer one.

- **A.8** If 'top sand' is between 2 and 3 m, the lithologic distribution of the overlying soft sediments determine if the sediment site-response class will be II, II or IV. Examples of HVSR-curves with 'top sand' between 2 and 3 m show peaks for certain lithological successions, forming a resonating layer. Class II is assigned if the overlying sediments contain more than 60% sand. Class III is assigned if the overlying sediments are mainly composed of clayey sand sandy clay; and class IV if clay and peat dominate. We do not elaborate on the exact percentages tot decide between Class III and IV. While testing the different criteria, this step appeared to be quite sensitive, and needed the implementation of several exceptions to the general rule.

- **A.9** If 'top sand' is larger than 3 m, the approach is basically the same as in **A.8**. Class II is assigned if the overlying sediments contain more that 60% sand. However, the exact criteria to decide between class III and IV differ from those in **A.8**.

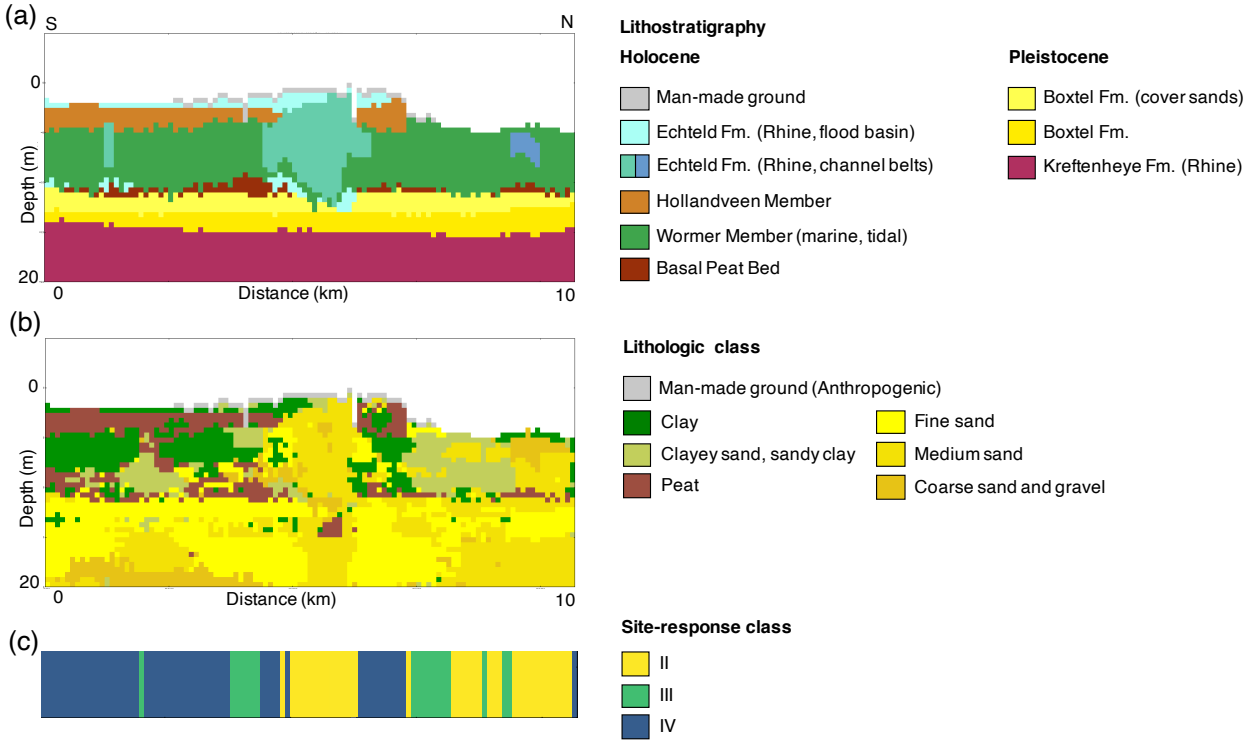

Figure C1. Cross-section through the GeoTOP voxel model: a) lithostratigraphy, b) lithologic class and c) corresponding sediment site-response class. The cross-section runs S-N through the city of Alphen aan den Rijn, situated on a sandy Holocene channel belt of the river Oude Rijn ('Old Rhine'). For location see Figure 13b). Class III and IV appear where soft, Holocene sediments (clay and peat) are overlying stiff Pleistocene deposits (sand). However, where Holocene sediments are sandy, such as in the channel belt in the center of the cross-section, Class II occurs.

Code and data availability. The data for the compilation of the site-response zonation map can be downloaded from the KNMI Data Platform: https://dataplatform.knmi.nl/dataset/seismic-site-response-zonation-map-1-0.

Author contributions. Janneke van Ginkel: method development, data analysis, construction of the map and underlying criteria, writing of manuscript with input from all co-authors. Elmer Ruigrok: daily advisor, input on data analysis method and results, performed text input.

Jan Stafleu: provided the GeoTOP and NL3D data, supported and quality checked the voxel-stack analysis and advised on the criteria for the construction of the site-response zonation map and performed text input. Rien Herber: promotor, initiator of this research project, advisor, method development, final text editor.

Competing interests. The authors declare no competing interests.

Acknowledgements. The authors thank the two reviewers for their valuable suggestions. This work is funded by EPI Kenniscentrum. Ambient noise and earthquake recordings were provided by KNMI and are publicly available through the website (http://rdsa.knmi.nl/dataportal). Figures are produced in Matlab. We would like to thank Deltares for the use of the SCPT data and lithological interpretations and TNO for the use of the 3D geological models and maps.

References

Akkar, S., Sandıkkaya, M., and Bommer, J. J.: Empirical ground-motion models for point-and extended-source crustal earthquake scenarios in Europe and the Middle East, Bulletin of earthquake engineering, 12, 359–387, 2014.

Albarello, D. and Lunedei, E.: Combining horizontal ambient vibration components for H/V spectral ratio estimates, Geophysical Journal International, 194, 936–951, 2013.

Bard, P.-Y.: Microtremor measurements: a tool for site effect estimation, in: Proceeding of the Second International Symposium on the Effects of Surface Geology on Seismic Motion, vol. 3, pp. 1251–1279, AA Balkema Rotterdam, 1998.

Bard, P.-Y.: Extracting information from ambient seismic noise: the SESAME project (Site EffectS assessment using AMbient Excitations), European Project EVG1-CT-2000-00026 SESAME, 2002.

Bard, P.-Y., Campillo, M., Chavez-Garcia, F., and Sanchez-Sesma, F.: The Mexico earthquake of September 19, 1985—A theoretical investigation of large-and small-scale amplification effects in the Mexico City Valley, Earthquake spectra, 4, 609–633, 1988.

Bazzurro*, P. and Cornell, C. A.: Nonlinear soil-site effects in probabilistic seismic-hazard analysis, Bulletin of the seismological society of America, 94, 2110–2123, 2004.

Beets, D. J. and van der Spek, A. J.: The Holocene evolution of the barrier and the back-barrier basins of Belgium and the Netherlands as a function of late Weichselian morphology, relative sea-level rise and sediment supply, Netherlands Journal of Geosciences, 79, 3–16, 2000.

Bindi, D., Massa, M., Luzi, L., Ameri, G., Pacor, F., Puglia, R., and Augliera, P.: Pan-European ground-motion prediction equations for the average horizontal component of PGA, PGV, and 5%-damped PSA at spectral periods up to 3.0 s using the RESORCE dataset, Bulletin of Earthquake Engineering, 12, 391–430, 2014.

Bommer, J. J., Stafford, P. J., Edwards, B., Dost, B., van Dedem, E., Rodriguez-Marek, A., Kruiver, P., van Elk, J., Doornhof, D., and Ntinalexis, M.: Framework for a ground-motion model for induced seismic hazard and risk analysis in the Groningen gas field, the Netherlands, Earthquake Spectra, 33, 481–498, 2017.

Bonnefoy-Claudet, S., Cornou, C., Bard, P.-Y., Cotton, F., Moczo, P., Kristek, J., and Donat, F.: H/V ratio: a tool for site effects evaluation. Results from 1-D noise simulations, Geophysical Journal International, 167, 827–837, 2006a.

Bonnefoy-Claudet, S., Cotton, F., and Bard, P.-Y.: The nature of noise wavefield and its applications for site effects studies: A literature review, Earth-Science Reviews, 79, 205–227, 2006b.

Bonnefoy-Claudet, S., Köhler, A., Cornou, C., Wathelet, M., and Bard, P.-Y.: Effects of Love waves on microtremor H/V ratio, Bulletin of the Seismological Society of America, 98, 288–300, 2008.

Bonnefoy-Claudet, S., Baize, S., Bonilla, L. F., Berge-Thierry, C., Pasten, C., Campos, J., Volant, P., and Verdugo, R.: Site effect evaluation in the basin of Santiago de Chile using ambient noise measurements, Geophysical Journal International, 176, 925–937, 2009.

Boore, D. M.: Simulation of ground motion using the stochastic method, Pure and applied geophysics, 160, 635–676, 2003.

Borcherdt, R. D.: Effects of local geology on ground motion near San Francisco Bay, Bulletin of the Seismological Society of America, 60, 29–61, 1970.

Borcherdt, R. D.: Estimates of site-dependent response spectra for design (methodology and justification), Earthquake spectra, 10, 617–653, 1994.

Bourne, S., Oates, S., van Elk, J., and Doornhof, D.: A seismological model for earthquakes induced by fluid extraction from a subsurface reservoir, Journal of Geophysical Research: Solid Earth, 119, 8991–9015, 2014.

Bradley, B. A.: Strong ground motion characteristics observed in the 4 September 2010 Darfield, New Zealand earthquake, Soil Dynamics and Earthquake Engineering, 42, 32–46, 2012.

Buijze, L., Van Den Bogert, P. A., Wassing, B. B., Orlic, B., and Ten Veen, J.: Fault reactivation mechanisms and dynamic rupture modelling of depletion-induced seismic events in a Rotliegend gas reservoir, Netherlands Journal of Geosciences, 96, s131–s148, 2017.

Busschers, F., Kasse, C., Van Balen, R., Vandenberghe, J., Cohen, K., Weerts, H., Wallinga, J., Johns, C., Cleveringa, P., and Bunnik, F.: Late Pleistocene evolution of the Rhine-Meuse system in the southern North Sea basin: imprints of climate change, sea-level oscillation and glacio-isostacy, Quaternary Science Reviews, 26, 3216–3248, 2007.

Camelbeeck, T. and Van Eck, T.: The 1992 Roermond earthquake, the Netherlands, and its aftershocks T. Camelbeeck", T. van Eck ", R. Pelzing", L. Ahorner ", J. Loohuis", HW Haak°,* P. Hoang-Trong° & D. Hollnack", Geologie en Mijnbouw, 73, 181–197, 1994.

Castellaro, S., Mulargia, F., and Rossi, P. L.: VS30: Proxy for seismic amplification?, seismological research letters, 79, 540–543, 2008.

CEN, E. et al.: 1 Design of structures for earthquake resistance–Part 1: General rules seismic actions and rules for buildings, European Committee for Standardization, 2004.

Convertito, V., De Matteis, R., Cantore, L., Zollo, A., Iannaccone, G., and Caccavale, M.: Rapid estimation of ground-shaking maps for seismic emergency management in the Campania Region of southern Italy, Natural hazards, 52, 97, 2010.

De Gans, W.: Quaternary Geology of the Netherlands, In Geology of the Netherlands by Wong, Th.E., Batjes, D.A.J. and De Jager, J. (eds.), pp. 173–195, 2007.

Dost, B., Ruigrok, E., and Spetzler, J.: Development of seismicity and probabilistic hazard assessment for the Groningen gas field, Netherlands Journal of Geosciences, 96, s235–s245, 2017.

Fäh, D., Kind, F., and Giardini, D.: A theoretical investigation of average H/V ratios, Geophysical Journal International, 145, 535–549, 2001.

Falcone, G., Acunzo, G., Mendicelli, A., Mori, F., Naso, G., Peronace, E., Porchia, A., Romagnoli, G., Tarquini, E., and Moscatelli, M.: Seismic amplification maps of Italy based on site-specific microzonation dataset and one-dimensional numerical approach, Engineering Geology, p. 106170, 2021.

Field, E. H. and Jacob, K. H.: A comparison and test of various site-response estimation techniques, including three that are not reference-site dependent, Bulletin of the seismological society of America, 85, 1127–1143, 1995.

Gallipoli, M., Calamita, G., Tragni, N., Pisapia, D., Lupo, M., Mucciarelli, M., Stabile, T., Perrone, A., Amato, L., Izzi, F., et al.: Evaluation of soil-building resonance effect in the urban area of the city of Matera (Italy), Engineering Geology, 272, 105 645, 2020.

Gallipoli, M. R. and Mucciarelli, M.: Comparison of site classification from VS 30, VS 10, and HVSR in Italy, Bulletin of the Seismological Society of America, 99, 340–351, 2009.

Gariel, J., Horrent, C., Jongmans, D., and Camelbeeck, T.: Strong ground motion computation of the 1992 Roermond earthquake, the Netherlands, from linear methods using locally recorded aftershocks, Geologie en Mijnbouw, 73, 315–315, 1995.

Geluk, M., Duin, E. T., Dusar, M., Rijkers, R., Van den Berg, M., and Van Rooijen, P.: Stratigraphy and tectonics of the Roer Valley Graben, Geologie en Mijnbouw, 73, 129–129, 1995.

Gouw, M. and Erkens, G.: Architecture of the Holocene Rhine-Meuse delta (the Netherlands)-a result of changing external controls, Netherlands Journal of Geosciences, 86, 23–54, 2007.

Guillier, B., Chatelain, J.-L., Bonnefoy-Claudet, S., and Haghshenas, E.: Use of ambient noise: From spectral amplitude variability to H/V stability, Journal of Earthquake Engineering, 11, 925–942, 2007.

Gunnink, J., Maljers, D., Van Gessel, S., Menkovic, A., and Hummelman, H.: Digital Geological Model (DGM): a 3D raster model of the subsurface of the Netherlands, Netherlands Journal of Geosciences, 92, 33–46, 2013.

Hijma, M. P., Cohen, K. M., Hoffmann, G., Van der Spek, A. J., and Stouthamer, E.: From river valley to estuary: the evolution of the Rhine mouth in the early to middle Holocene (western Netherlands, Rhine-Meuse delta), Netherlands Journal of Geosciences, 88, 13–53, 2009.

Hinzen, K.-G., Reamer, S. K., and Fleischer, C.: Seismicity in the Northern Rhine Area (1995–2018), Journal of Seismology, pp. 1–17, 2020.

Hofman, L., Ruigrok, E., Dost, B., and Paulssen, H.: A shallow seismic velocity model for the Groningen area in the Netherlands, Journal of Geophysical Research: Solid Earth, 122, 8035–8050, 2017.

Houtgast, R. and Van Balen, R.: Neotectonics of the Roer Valley rift system, the Netherlands, Global and Planetary Change, 27, 131–146, 2000.

Joyner, W. B. and Boore, D. M.: Peak horizontal acceleration and velocity from strong-motion records including records from the 1979 Imperial Valley, California, earthquake, Bulletin of the seismological Society of America, 71, 2011–2038, 1981.

KNMI: Netherlands Seismic and Acoustic Network, Royal Netherlands Meteorological Institute (KNMI), Other/Seismic Network, https://doi.org/https://doi.org/10.21944/e970fd34-23b9-3411-b366-e4f72877d2c5, 1993.

Kokusho, T. and Sato, K.: Surface-to-base amplification evaluated from KiK-net vertical array strong motion records, Soil Dynamics and Earthquake Engineering, 28, 707–716, 2008.

Konno, K. and Ohmachi, T.: Ground-motion characteristics estimated from spectral ratio between horizontal and vertical components of microtremor, Bulletin of the Seismological Society of America, 88, 228–241, 1998.

Kruiver, P. P., van Dedem, E., Romijn, R., de Lange, G., Korff, M., Stafleu, J., Gunnink, J. L., Rodriguez-Marek, A., Bommer, J. J., van Elk, J., et al.: An integrated shear-wave velocity model for the Groningen gas field, the Netherlands, Bulletin of Earthquake Engineering, pp. 1–26, doi: 10.1007/s10518-017-0105-y, 2017a.

Kruiver, P. P., Wiersma, A., Kloosterman, F. H., de Lange, G., Korff, M., Stafleu, J., Busschers, F. S., Harting, R., Gunnink, J. L., Green, R. A., et al.: Characterisation of the Groningen subsurface for seismic hazard and risk modelling, Netherlands Journal of Geosciences, 96, s215–s233, 2017b.

Kwok, A. O., Stewart, J. P., and Hashash, Y. M.: Nonlinear ground-response analysis of Turkey Flat shallow stiff-soil site to strong ground motion, Bulletin of the Seismological Society of America, 98, 331–343, 2008.

Lachetl, C. and Bard, P.-Y.: Numerical and theoretical investigations on the possibilities and limitations of Nakamura's technique, Journal of Physics of the Earth, 42, 377–397, 1994.

Lee, V. W. and Trifunac, M. D.: Should average shear-wave velocity in the top 30 m of soil be used to describe seismic amplification?, Soil Dynamics and Earthquake Engineering, 30, 1250–1258, 2010.

Lermo, J. and Chavez-Garcia, F. J.: Site effect evaluation using spectral ratios with only one station, Bulletin of the seismological society of America, 83, 1574–1594, 1993.

Lunedei, E. and Malischewsky, P.: A review and some new issues on the theory of the H/V technique for ambient vibrations, in: Perspectives on European Earthquake Engineering and Seismology, pp. 371–394, 2015.

Majer, E. L., Baria, R., Stark, M., Oates, S., Bommer, J., Smith, B., and Asanuma, H.: Induced seismicity associated with enhanced geothermal systems, Geothermics, 36, 185–222, 2007.

Mena, B., Wiemer, S., and Bachmann, C.: Building robust models to forecast the induced seismicity related to geothermal reservoir enhancement, Bulletin of the Seismological Society of America, 103, 383–393, 2013.

Mignan, A., Landtwing, D., Kästli, P., Mena, B., and Wiemer, S.: Induced seismicity risk analysis of the 2006 Basel, Switzerland, Enhanced Geothermal System project: Influence of uncertainties on risk mitigation, Geothermics, 53, 133–146, 2015.

Molnar, S., Cassidy, J., Castellaro, S., Cornou, C., Crow, H., Hunter, J., Matsushima, S., Sánchez-Sesma, F., and Yong, A.: Application of microtremor horizontal-to-vertical spectral ratio (MHVSR) analysis for site characterization: State of the art, Surveys in Geophysics, 39, 613–631, 2018.

Nakamura, Y.: A method for dynamic characteristics estimation of subsurface using microtremor on the ground surface, Railway Technical Research Institute, Quarterly Reports, 30, 1989.

Nakamura, Y.: What Is the Nakamura Method?, Seismological Research Letters, 90, 1437–1443, https://doi.org/10.1785/0220180376, 2019.

Nakata, N., Snieder, R., Kuroda, S., Ito, S., Aizawa, T., and Kunimi, T.: Monitoring a building using deconvolution interferometry. I: Earthquake-data analysis, Bulletin of the Seismological Society of America, 103, 1662–1678, 2013.

Nogoshi, M. and Igarashi, T.: On the propagation characteristics of microtremors, J. Seism. Soc. Japan, 23, 264–280, 1970.

Noorlandt, R., Kruiver, P. P., de Kleine, M. P., Karaoulis, M., de Lange, G., Di Matteo, A., von Ketelhodt, J., Ruigrok, E., Edwards, B., Rodriguez-Marek, A., et al.: Characterisation of ground motion recording stations in the Groningen gas field, Journal of seismology, 22, 605–623, 2018.

Panzera, F., Bergamo, P., and Fäh, D.: Canonical Correlation Analysis Based on Site-Response Proxies to Predict Site-Specific Amplification Functions in Switzerland, Bulletin of the Seismological Society of America, 2021.

Paulssen, H., Dost, B., and Van Eck, T.: The April 13, 1992 earthquake of Roermond (The Netherlands); first interpretation of the NARS seismograms, Geologie en Mijnbouw, 71, 91–91, 1992.

Peeters, J., Busschers, F., Stouthamer, E., Bosch, J., Van den Berg, M., Wallinga, J., Versendaal, A., Bunnik, F., and Middelkoop, H.: Sedimentary architecture and chronostratigraphy of a late Quaternary incised-valley fill: a case study of the late Middle and Late Pleistocene Rhine system in the Netherlands, Quaternary Science Reviews, 131, 211–236, 2016.

Perron, V., Gélis, C., Froment, B., Hollender, F., Bard, P.-Y., Cultrera, G., and Cushing, E. M.: Can broad-band earthquake site responses be predicted by the ambient noise spectral ratio? Insight from observations at two sedimentary basins, Geophysical Journal International, 215, 1442–1454, 2018.

Pilz, M., Parolai, S., Leyton, F., Campos, J., and Zschau, J.: A comparison of site response techniques using earthquake data and ambient seismic noise analysis in the large urban areas of Santiago de Chile, Geophysical Journal International, 178, 713–728, 2009.

Poggi, V., Edwards, B., and Fäh, D.: Derivation of a reference shear-wave velocity model from empirical site amplification, Bulletin of the Seismological Society of America, 101, 258–274, 2011.

Rodriguez-Marek, A., Kruiver, P. P., Meijers, P., Bommer, J. J., Dost, B., van Elk, J., and Doornhof, D.: A Regional Site-Response Model for the Groningen Gas Field, Bulletin of the Seismological Society of America, 107, 2067–2077, 2017.

Rondeel, H., Batjes, D., and Nieuwenhuijs, W.: Synopsis: Petroleum geology of the Netherlands—1993, Geology of gas and oil under the Netherlands: The Royal Geological and Mining Society of The Netherlands, pp. S3–S20, 1996.

Schokker, J.: Geologische overzichtskaart van Nederland, TNO Bouw en Ondergrond (Utrecht), 2010.

Stafleu, J., Maljers, D., Gunnink, J., Menkovic, A., and Busschers, F.: 3D modelling of the shallow subsurface of Zeeland, the Netherlands, Netherlands Journal of Geosciences, 90, 293–310, 2011.

Stafleu, J., Maljers, D., Busschers, F. S., Schokker, J., Gunnink, J. L., and Dambrink, R. M.: Models Created as 3-D Cellular Voxel Arrays, Applied Multidimensional Geological Modeling: Informing sustainable human interactions with the shallow subsurface, pp. 247–271, https://doi.org/10.1002/9781119163091.ch11, 2021.

Van den Berg, M. and Beets, D.: Saalian glacial deposits and morphology in The Netherlands, Tills and Glaciotectonics. Balkema, Rotterdam, pp. 235–251, 1987.

Van der Meulen, M., Doornenbal, J., Gunnink, J., Stafleu, J., Schokker, J., Vernes, R., Van Geer, F., Van Gessel, S., Van Heteren, S., Van Leeuwen, R., et al.: 3D geology in a 2D country: perspectives for geological surveying in the Netherlands, Netherlands Journal of Geosciences, 92, 217–241, 2013.

van Ginkel, J., Ruigrok, E., and Herber, R.: Assessing soil amplifications in Groningen, the Netherlands, First Break, 37, 33–38, 2019.

van Ginkel, J., Ruigrok, E., and Herber, R.: Using horizontal-to-vertical spectral ratios to construct shear-wave velocity profiles, Solid Earth, 11, 2015–2030, https://doi.org/10.5194/se-11-2015-2020, 2020.

van Thienen-Visser, K. and Breunese, J.: Induced seismicity of the Groningen gas field: history and recent developments, The Leading Edge, 34, 664–671, 2015.

Wapenaar, K., Slob, E., Snieder, R., and Curtis, A.: Tutorial on seismic interferometry: Part 2—Underlying theory and new advances, Geophysics, 75, 75A211–75A227, 2010.

Wassing, B., Dost, B., and Vermillion, N. P.: Seismisch hazard van geinduceerde aardbevingen: integratie van deelstudies, 2012.

Weatherill, G., Kotha, S. R., and Cotton, F.: Re-thinking site amplification in regional seismic risk assessment, Earthquake Spectra, 36, 274–297, 2020.

Wills, C., Petersen, M., Bryant, W., Reichle, M., Saucedo, G., Tan, S., Taylor, G., and Treiman, J.: A site-conditions map for California based on geology and shear-wave velocity, Bulletin of the Seismological Society of America, 90, S187–S208, 2000.

Zagwijn, W.: The Netherlands during the Tertiary and the Quaternary: a case history of coastal lowland evolution, in: Coastal Lowlands, pp. 107–120, Springer, 1989.